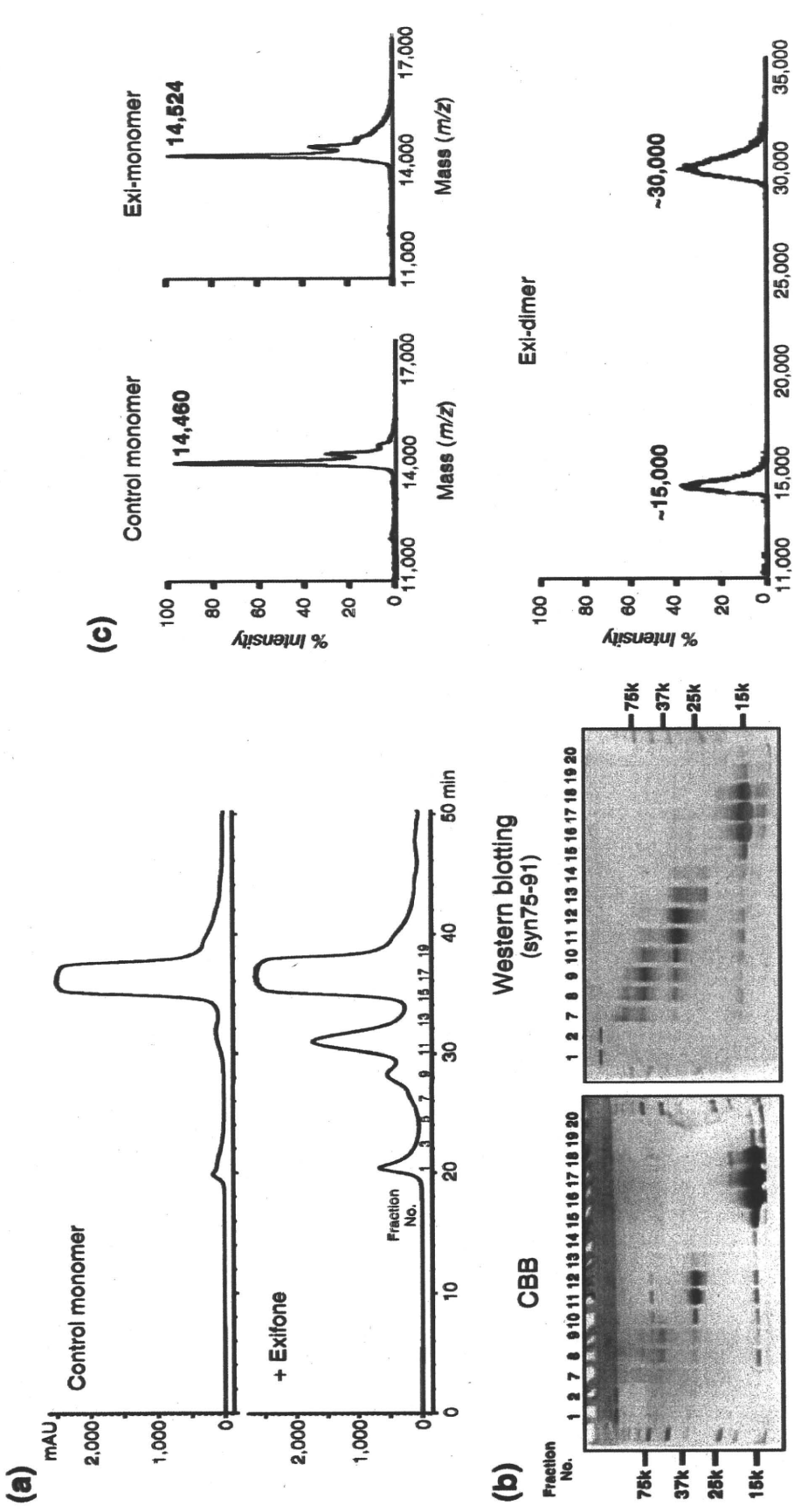

Fig. 2. Isolation and characterization of exifone-bound α-synucleins. (a) Separation of exifone-treated α-synuclein monomer and dimer by gel-filtration chromatography (detection: absorbance at 214 nm). (b) SDS-PAGE of fractions separated by gel-filtration chromatography (Coomassie brilliant blue staining and Western blotting). Pooled fractions 11–12 and 16–18 were used as Exi-dimer and Exi-monomer, respectively. (c) Partial MALDI-TOF MS spectra of α-synuclein monomer (control), Exi-monomer, and Exi-dimer.

molecules of exifone per α-synuclein monomer, while Exi-monomer contains one exifone molecule per α-synuclein chain (**Supplementary Fig. S1**).

For the identification of the modification (corresponding to a molecular mass of 64 Da) found in the Exi-monomer, α-synuclein was incubated with various concentrations of exifone (0, 0.2, 0.5, 1, and 2 mM) and the resulting samples were analyzed by MS (**Supplementary Fig. S2**). The molecular mass of α-synuclein increased in an exifone concentration-dependent manner and reached 14,528 Da (**Supplementary Fig. S2a and b**). A similar increase in molecular mass was reported in the presence of H_2O_2, which oxidized methionine residues to methionine sulfoxide.[14] Methionine oxidation is known to increase mass by 16 Da. α-Synuclein has four methionine residues, Met1, Met5, Met116, and Met127, and thus the oxidation of all the methionine residues would result in an increase in mass of 64 Da (**Supplementary Fig. S3c**). Indeed, α-synuclein incubated with various concentrations of H_2O_2 showed a concentration-dependent increase in molecular mass of up to 14,533 Da (**Supplementary Fig. S3a and b**), similar to that seen in the case of exifone. These results strongly suggest that all the methionine residues of Exi-monomer were oxidized to methionine sulfoxide.

Peptide mapping of inhibitor-induced α-synuclein dimer and monomer

In order to confirm the oxidation of methionine, control α-synuclein, Exi-monomer, Exi-dimer, and H_2O_2-treated α-synuclein monomer were digested with trypsin, and the resulting peptide mixtures were analyzed by reverse-phase HPLC (**Fig. 3a**). The elution patterns of peptides derived from Exi-monomer and Exi-dimer exhibited different profiles compared with that of control α-synuclein. Peaks 5 and 10 in the map of control α-synuclein were absent in the maps of Exi-monomer and Exi-dimer. Instead, peaks 11–18 newly appeared in the maps of Exi-monomer and Exi-dimer. The patterns of Exi-monomer and Exi-dimer were similar to those of α-synuclein oxidized with H_2O_2. All the peaks were analyzed by MS and the results are summarized in **Fig. 3b**. Peaks 5 and 10 were identified as Met1–Lys6 (containing two methionines, Met1 and Met5) and Asn103–Ala140 (containing Met116 and Met127), respectively. In the case of Exi-monomer or Exi-dimer, peaks 11, 15, and 19 were identified as Met1–Lys6 including two oxidized methionines. Peaks 12, 16, and 20 were identified as Asn103–Ala140 including oxidized Met116 and Met127. Peaks 13, 14, 16, and 17 were derived from Asn103–Ala140 oxidized at either Met116 or Met127. Similar results were obtained for dopamine-bound dimer and monomer (data not shown). These results clearly indicate that the inhibitors exifone and dopamine have the ability to oxidize methionine residues on α-synuclein. It is established that α-synuclein assembly was inhibited by exifone at low micromolar range (IC_{50}=2.5 μM),[3] and methionine sulfoxide could not be detected at a low concentration of exifone (data not shown). These findings suggest that the stabilization of intermediate oligomers by small molecules is responsible for the inhibition of filament formation, and oxidation of methionine does not seem to play a major role in inhibition.

No covalent inhibitor–peptide adducts or cross-linked peptides were detected in the peptide mapping experiments, indicating that the inhibitors bind noncovalently to α-synuclein and that α-synuclein dimer is formed in a noncovalent fashion. These observations are consistent with the results of MALDI MS analysis of Exi-monomer, which showed no inhibitor adducts (**Fig. 2c**). Our extensive liquid chromatography–electrospray ionization MS analysis also did not show the covalent inhibitor adducts or α-synuclein dimer (data not shown). Further, more detailed biochemical studies to investigate the modes of inhibitor binding and dimerization are currently in progress.

Characterization of exifone-binding regions in α-synuclein

Exifone is an antioxidant and thus can be detected by redox-cycling staining, which is a well-established method for detecting quinoproteins.[15] As expected, Exi-dimer and Exi-monomer were stained as purple bands by redox-cycling staining due to nitroblue tetrazolium (NBT) reduction to formazan (**Fig. 4a**), while untreated control α-synuclein showed no staining. This result shows that redox-cycling staining is useful for examining the exifone-binding regions in α-synuclein. In order to determine the binding region of exifone and the regions involved in the dimerization, Exi-dimer was digested with endoproteinase Asp-N and the resulting peptides were detected with silver or redox-cycling staining. Asp-N digestion of Exi-dimer gave two major fragments, corresponding to molecular masses of 20 kDa (no. 1) and 16 kDa (no. 2), on SDS-PAGE after silver staining (**Fig. 4b**). These two bands were positive for redox-cycling staining. Since α-synuclein monomer migrates at 15 kDa, these fragments represent dimeric peptides stabilized by exifone. α-Synuclein has six aspartic acid residues (Asp2, Asp98, Asp115, Asp119, Asp121, and Asp135). Immunoblot analysis with a panel of site-specific anti-α-synuclein antibodies (**Fig. 5**) suggested that the 20-kDa fragment contains the dimerized N-terminal fragment Met1–Met97 of α-synuclein (cleaved at the N-terminus of Asp98). The 16-kDa fragment was also labeled with antibodies to the N-terminal and central portions of α-synuclein (residues 1–50). It has been reported that Asp-N cleaves peptide bonds N-terminal to glutamate as well as aspartate residues.[16,17] Glu57 and/or Glu61 are found in the middle of α-synuclein and are candidate Asp-N cleavage sites to produce the 16-kDa fragment. The reactivity of anti-α-synuclein antibodies and the relaxed specificity of Asp-N indicate that the 16-kDa fragment corresponds to a dimer composed of Met1–Ala56/Lys60. These results suggest that the N-

terminal region (1–60) of α-synuclein is involved in the dimerization and exifone binding. This is in contrast with a previous report by Norris *et al.*, in which they suggested that dopamine inhibited the aggregation of α-synuclein by binding to the C-terminal residues 125–129 (i.e., YEMPS) and stabilizing the soluble oligomers.[6] The discrepancy might be due to the fact that they analyzed the dopamine-binding sites by using deletion mutants lacking the C-terminal regions and did not use full-length α-synucleins.

High-resolution NMR spectra of inhibitor-bound α-synuclein monomer and dimer

In order to characterize the behavior of α-synuclein monomer and dimer formed in the presence of polyphenolic compounds, we conducted a structural analysis of inhibitor-bound α-synuclein monomer and dimer using ultra-high-field NMR spectroscopy. NMR signals of backbone amides constitute excellent probes to provide maps of the interacting sites and to examine the effects of modifications.[13] **Fig. 6**a and b shows the ^{1}H–^{15}N heteronuclear single quantum coherence (HSQC) spectra of uniformly ^{15}N-labeled Exi-monomer and Exi-dimer, as well as control monomer, recorded at a proton observation frequency of 920 MHz. The amide resonances of Exi-monomer and Exi-dimer were assigned by comparing the NMR spectral data with those of control α-synuclein monomer. Little chemical shift difference was detected between Exi-monomer and control monomer for most observed peaks, except for the signals corresponding

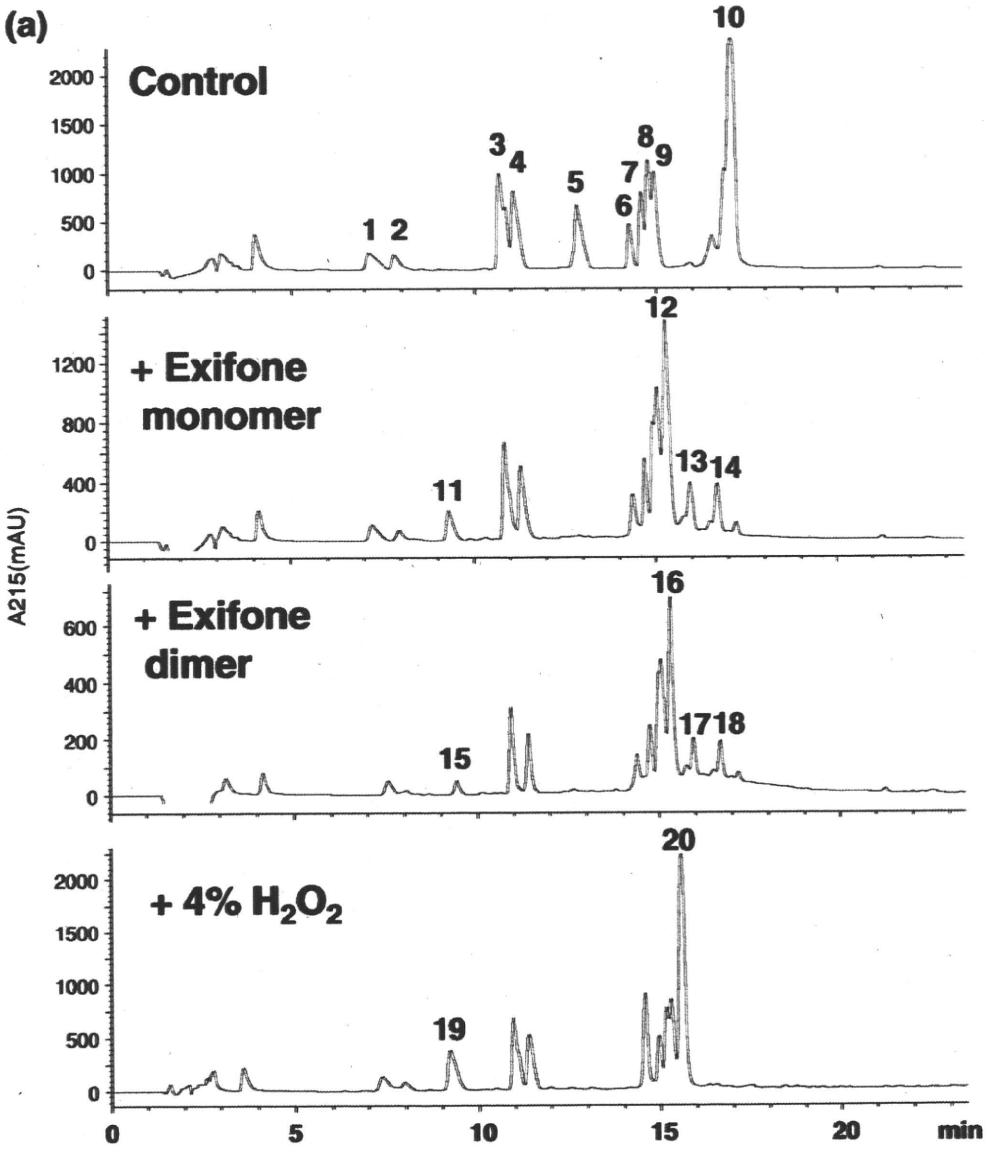

Fig. 3. Tryptic peptide mapping and MS analysis of α-synucleins. (a) Reverse-phase HPLC patterns of monomeric α-synuclein (control), Exi-monomer, Exi-dimer, and H_2O_2-treated α-synuclein monomer. (b) Observed masses and peak assignments of the peptides separated on a reverse-phase column. Oxidation of methionine residues was observed in Exi-monomer and Exi-dimer, as well as H_2O_2-treated α-synuclein monomer.

(b)

Peak No.	$(M+H)^+$ Observed	$(M+H)^+$ Calculated	Assignment
1	830.6 873.5 1072.6	830.4 873.4 1072.5	QGVAEAAGK (24-32) EGVVAAAEK (13-21) AKEGVVAAAEK (11-21)
2	1180.7 1295.8 1524.8	1180.6 1295.6 1524.8	TKEGVLYVGSK (33-43) EGVVHGVATVAEK (46-58) TKEGVVHGVATVAEK (44-58)
3	951.5	951.5	EGVLYVGSK (35-43)
4	1295.7	1295.6	EGVVHGVATVAEK (46-58)
5	770.5	770.3	MDVFMK (1-6)
6	1606.6	1606.8	TVEGAGSIAAATGFVKK (81-97)
7	2157.2	2157.1	TKEQVTNVGGAVVTGVTAVAQK (58-80)
8	1478.5	1478.7	TVEGAGSIAAATGFVK (81-96)
9	1928.0	1928.0	EQVTNVGGAVVTGVTAVAQK (61-80)
10	4295.0	4286.7	NEEGAPQEGILEDMPVDPDNAYEMPSEEGYQDYEPEA (103-140)
11	803.0	802.3.0	M*DVFM*K (1-6) (M*:methionine sulfoxide)
12	4322.0	4318.7	NEEGAPQEGILEDM*PVDPDNAYEM*PSEEGYQDYEPEA (103-140)
13	4311.0	4302.7	NEEGAPQEGILEDM#PVDPDNAYEM*PSEEGYQDYEPEA (103-140) (One of two methionine residues (M#) was oxidized)
14	4312.0	4302.7	NEEGAPQEGILEDM#PVDPDNAYEM#PSEEGYQDYEPEA (103-140)
15	802.0	802.3	M*DVFM*K (1-6)
16	4322.0	4318.7	NEEGAPQEGILEDM*PVDPDNAYEM*PSEEGYQDYEPEA (103-140)
17	4311.0	4302.7	NEEGAPQEGILEDM#PVDPDNAYEM*PSEEGYQDYEPEA (103-140)
18	4312.0	4302.7	NEEGAPQEGILEDM#PVDPDNAYEM#PSEEGYQDYEPEA (103-140)
19	803.0	802.3	M*DVFM*K (1-6)
20	4322.0	4318.7	NEEGAPQEGILEDM*PVDPDNAYEM*PSEEGYQDYEPEA (103-140)

Fig. 3 *(legend on previous page)*

to Met5, Met116, Met127, and their neighboring residues (**Fig. 6a**). The observed chemical shift differences are mostly attributable to the oxidation of methionine residues. The differences in peak intensities between Exi-monomer and control monomer were also generally small (**Fig. 6c**). These results indicate that the dynamical features of both synuclein monomers are almost the same, and methionine oxidation itself does not greatly influence the structural characteristics of α-synuclein.

It is noteworthy that significant reductions in signal intensity [I(Exi-dimer)/I(control monomer)< 0.8] were observed for the peaks originating from the N-terminal region (1–60) of Exi-dimer compared with the control monomer (**Fig. 6d**). This result shows that the N-terminal regions are involved in exifone-induced dimerization of α-synuclein, in accordance with the results obtained from Asp-N digestion of the Exi-dimer. The gradual reduction in the signal intensities might be explained by heterogeneous dimerization around the N-terminus. The observed reduction in signal intensity, in our case, was not due to chemical exchange between the inhibitor-free and inhibitor-bound states of α-synuclein, as had been suggested by Rao *et al.*,[10] because the inhibitor-induced dimer and monomer were each purified to homogeneity and free or exchangeable inhibitors were removed by gel-filtration column chromatography and buffer exchange. Similar NMR spectra were observed for dopamine- and gossypetin-induced dimers (**Supplementary Fig. S4**), indicating that the N-terminal dimerization modes induced by dopamine, exifone, and gossypetin are the same or at least very similar. On the other hand, the C-terminal portion of exifone-bound dimer was still predominantly random coil in character, as observed in the control monomeric α-synuclein. These

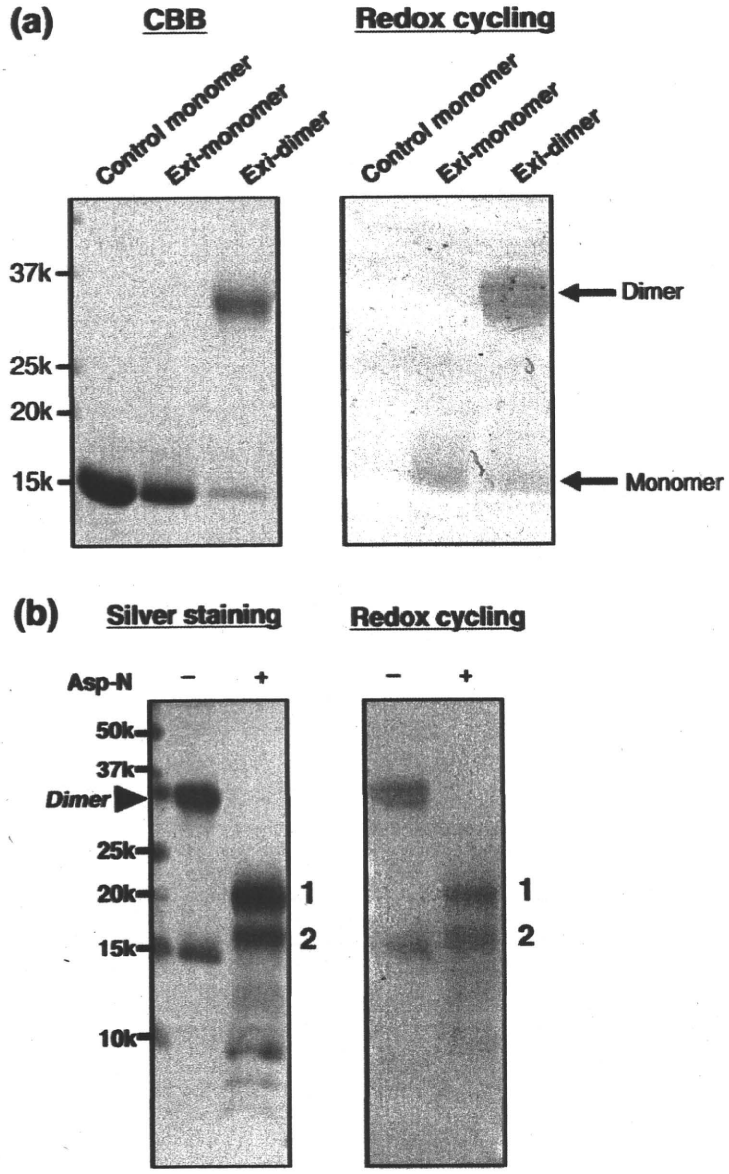

Fig. 4. Detection of exifone bound to α-synucleins by redox-cycling staining. (a) Control monomer, Exi-monomer, and Exi-dimer were stained with Coomassie brilliant blue (left) or by redox cycling (right). Exifone-bound α-synucleins were stained by redox cycling, appearing as purple-blue bands in the Exi-monomer and Exi-dimer lanes, due to NBT reduction to formazan (right). (b) Asp-N digestion of Exi-dimer. Exi-dimer was digested with endoproteinase Asp-N and the fragments were detected by silver staining (left) and redox staining (right). Two major bands corresponding to 20 kDa and 16 kDa (nos. 1 and 2, respectively) were positive for redox-cycling staining.

observations indicate the importance of the N-terminal region in α-synuclein assembly.

It is of note that three missense mutations in familial PD (A30P, E46K, and A53T) are located in the N-terminal region of α-synuclein. Recent NMR analyses suggest that these mutations may be altering the physicochemical properties of the protein, such as net charge (E46K) and secondary-structure propensity (A30P and A53T).[19] The binding of exifone, gossypetin, or dopamine to α-synuclein might also alter the net charge and/or secondary-structure propensity.

We did not observe the colloidal formation of exifone, gossypetin, or dopamine by electron microscopy (data not shown) as reported by Feng *et al.*[5] The discrepancy might be due to differences in the compounds used or differences in the proteins investigated. The inhibition mechanism of these three compounds seems rather specific because the N-terminal region was specifically involved in inhibitor binding, which is in contrast to the nonspecific colloidal inhibition.

In summary, we have characterized the inhibitor-bound α-synuclein dimer and showed that the N-terminal region (1–60) plays a key role in dimerization and inhibitor binding. Further studies are under way in our laboratory to elucidate the mechanisms of inhibitor-induced oligomer formation at atomic resolution.

Materials and Methods

Antibodies

Polyclonal antibodies were raised against synthetic peptides corresponding to residues 1–10, 11–20, 21–30, 31–40, 41–50, 51–60, 61–70, 75–91, and 131–140 of human α-synucleins, prepared as described previously.[12] Antibody

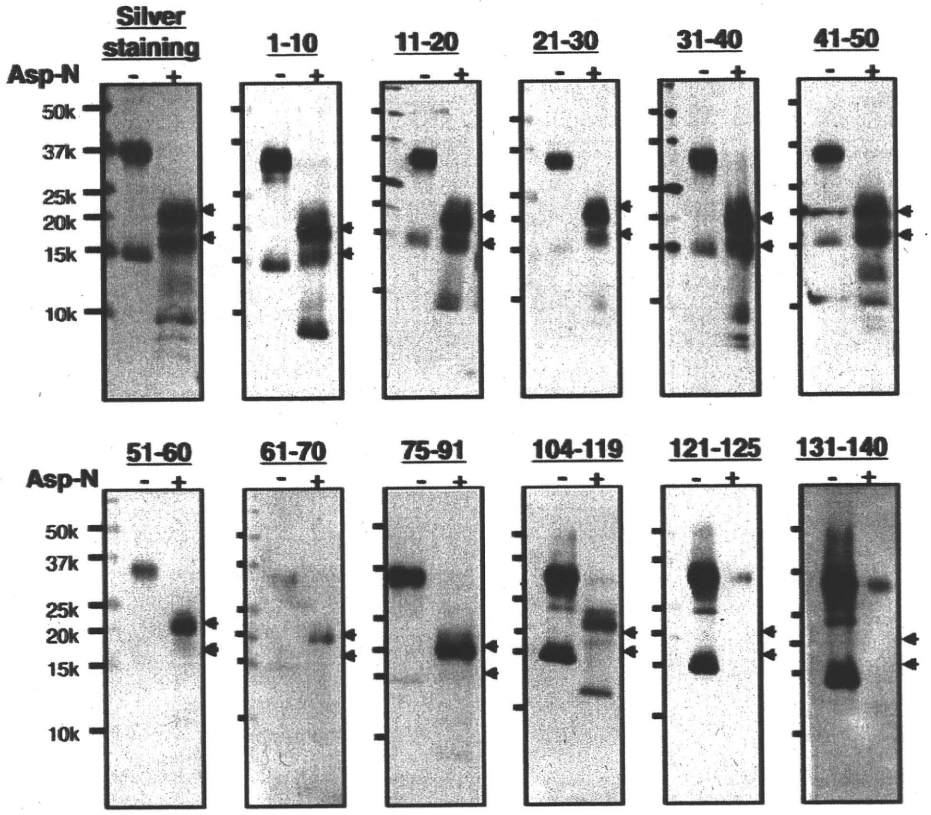

Fig. 5. Immunoblot analysis of Asp-N digests of Exi-dimer. Silver staining and immunoblots of Asp-N digests of Exi-dimer with a panel of anti-α-synuclein antibodies raised against nine peptides (corresponding to residues 1–10, 11–20, 21–30, 31–40, 41–50, 51–60, 61–70, 75–91, and 131–140).[12] Experimental details are given in **Materials and Methods**. Two major fragments (band nos. 1 and 2) were detected with silver staining (indicated with arrowheads). Fragment no. 1 was positive for antibodies to the N-terminal region, 1–97, and no. 2 was positive for antibodies to the N-terminal region, 1–50.

Syn259, which recognizes residues 104–119 of α-synuclein, was kindly provided by Dr. S. Nakajo. Monoclonal antibody Syn211, which recognizes residues 121–125 of α-synuclein, was purchased from Zymed.

Protein expression and purification

Expression of isotopically labeled α-synuclein was performed as described.[13] Human α-synuclein cDNA in bacterial expression plasmid pRK172 was used for production of isotopically labeled protein for NMR analyses.[20] Codon 136 was changed from TAC to TAT by site-directed mutagenesis to avoid cysteine misincorporation.[21] Uniformly ^{15}N-labeled α-synuclein was expressed in *Escherichia coli* BL21(DE3) cells grown in M9 minimal medium containing 1 g/L $[^{15}N]NH_4Cl$, while unlabeled α-synuclein was expressed using LB medium. Cell lysates were subjected to boiling and subsequently to ammonium sulfate precipitation. The precipitated α-synuclein was extensively dialyzed against 20 mM Tris–HCl (pH 8.0) and then purified with DEAE ion-exchange chromatography.

Preparation of inhibitor-bound α-synuclein monomers and dimers

Purified ^{15}N-labeled recombinant α-synuclein (9 mg/mL) was incubated with 2 mM inhibitor (exifone, gossypetin, or dopamine; see **Fig. 1**) for 30 days at 37 °C in 30 mM Tris–HCl containing 0.1% sodium azide. The samples were then centrifuged at 113,000*g* for 20 min. The supernatants were loaded on a Sephadex G-25 gel-filtration column to separate oligomers from unbound inhibitor. The eluates were fractionated on a Superdex 200 gel-filtration column (1 cm × 30 cm), eluted with 10 mM Tris–HCl (pH 7.5) containing 150 mM NaCl. Eluates were monitored at 215 nm. α-Synuclein monomer and dimer fractions were each concentrated and the concentrates were subjected to NMR analysis. Protein concentrations were determined using HPLC and bicinchoninic acid protein assay kit (Pierce).

Mass spectrometry

Samples were spotted on a sample plate and mixed with the matrix solutions, saturated sinapic acid (Fluka) or α-cyano-4-hydroxycinnamic acid (Fluka) in 50% acetonitrile/H_2O containing 0.1% (v/v) trifluoroacetic acid. Mass spectra were obtained by MALDI-TOF MS using a Voyager-DE Pro mass spectrometer (PerSeptive Biosystems).

Peptide mapping of H_2O_2-treated and inhibitor-bound α-synucleins

Inhibitor-bound α-synuclein monomer and dimer were prepared as described above. For methionine oxidation, α-synuclein monomer (7 mg/mL) was incubated with 0–4% H_2O_2 at room temperature for 20 min and then dialyzed

against 30 mM Tris–HCl (pH 7.5) to remove H_2O_2. To identify the modification, inhibitor-bound α-synuclein monomer and dimer, as well as H_2O_2-treated α-synuclein, were incubated with trypsin at 37 °C for 18 h at an enzyme-to-substrate ratio of 1:50 (mol/mol) in 30 mM Tris–HCl (pH 7.5). Digested peptide products were separated by reverse-phase HPLC on a Supersphere Select B column (2.1 × 125 mm; Merck) and analyzed by MALDI-TOF MS.

Determination of stoichiometry of exifone/α-synuclein complexes

The stoichiometry of exifone/α-synuclein complexes was determined by measuring the absorbance of exifone at 385 nm using a spectrophotometer (UV-1600 PC, Shimadzu Co). Exifone-bound monomeric and dimeric α-synucleins were isolated by gel-filtration chromatography as described above.

Redox-cycle staining

Samples were subjected to SDS-PAGE and transferred onto polyvinylidene fluoride membranes. The membranes were incubated in 0.24 mM NBT (Sigma), 2 M potassium glycinate solution (pH 10.0) in the dark for 16 h at room temperature and then dipped in 100 mM sodium borate (pH 10.0). Exifone-bound α-synuclein was specifically stained as purple-blue bands due to NBT reduction to formazan.

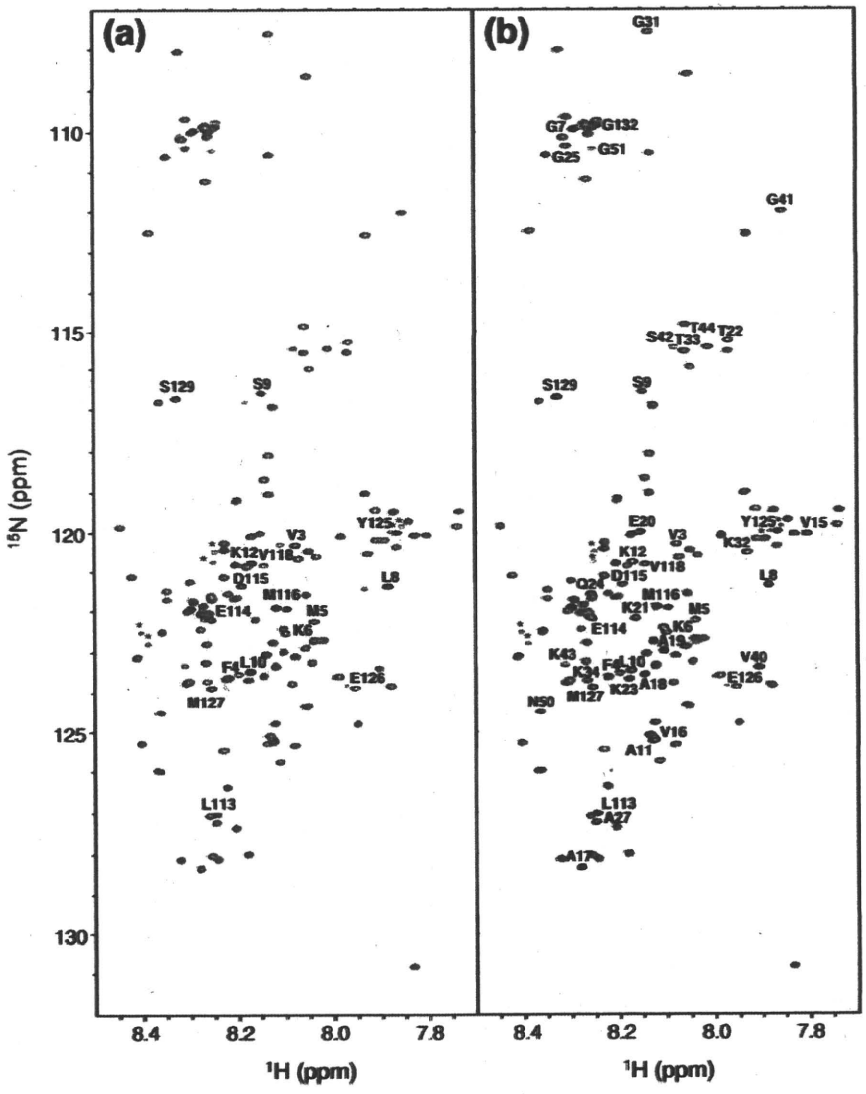

Fig. 6. NMR spectral comparison of exifone-bound ^{15}N-labeled α-synuclein dimer and control monomer. (a) ^{1}H–^{15}N HSQC spectra of ^{15}N-labeled Exi-monomer (red) and ^{15}N-labeled control monomer (black) recorded at a proton frequency of 920 MHz. (b) ^{1}H–^{15}N HSQC spectra of ^{15}N-labeled Exi-dimer (red) and ^{15}N-labeled control monomer (black). (c) Plot of the relative peak intensities, *I*(Exi-monomer)/*I*(monomer), of the HSQC cross-peaks in the Exi-monomer and control monomer *versus* the amino acid sequence of α-synuclein. (d) *I*(Exi-dimer)/*I*(monomer) of the HSQC cross-peaks in the Exi-dimer and control monomer. Signals derived from oxidized methionines and their neighboring residues (indicated with asterisks in a and b) were split and not taken into account. The peak splittings mostly reflect a mixture of *R* and *S* isomers of methionine sulfoxide.[18]

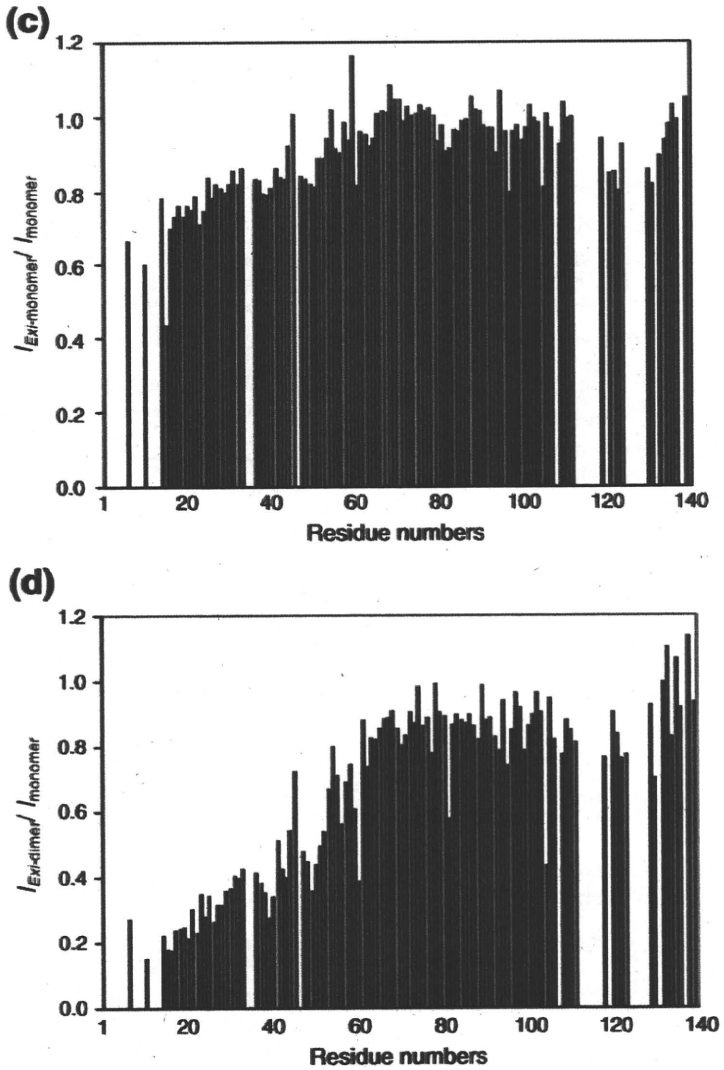

Fig. 6 *(legend on previous page)*

Asp-N digestion of α-synuclein dimer

α-Synuclein dimer (0.25 mg/mL) in 30 mM Tris–HCl (pH 7.5) was treated with 40 μg/mL of Asp-N (Roche) at 37 °C for 1 h. The reaction was stopped by adding 2× SDS sample buffer [4% SDS, 0.16 M Tris–HCl (pH 6.8), 30% glycerol] and the solution was boiled for 5 min. The samples were loaded onto 15% Tris/tricine SDS-PAGE gel, and the digested products were detected by silver staining (kit from Wako), immunoblotting, and redox-cycling staining. For immunoblotting, SDS-PAGE gels were blotted onto polyvinylidene fluoride membranes, blocked with 3% gelatin/phosphate-buffered saline, and incubated overnight at room temperature with anti-α-synuclein antibody in 10% FBS/phosphate-buffered saline. After washing, the blots were incubated for 2 h at room temperature with biotinylated secondary antibody (1:500) (Vector Laboratories). Following further washing, the blots were incubated with peroxidase-labeled avidin–biotin (Vector laboratories) for 30 min at room temperature and developed with $NiCl_2$-enhanced diaminobenzidine (Sigma).

NMR measurements

The samples for NMR experiments were prepared at a concentration of 0.1–1.0 mM in 90% H_2O/10% D_2O (v/v), 10 mM sodium phosphate buffer, and 100 mM NaCl at pH 7.0. NMR experiments were performed at 10 °C using a JEOL JNM-ECA920 spectrometer equipped with a 5-mm triple resonance probe. Backbone assignments of α-synuclein monomer were achieved by means of standard triple resonance experiments, as described previously.[13] The samples were checked by SDS-PAGE before and after NMR measurements, and it was confirmed that aggregation of inhibitor-bound α-synuclein monomer and dimer did not occur under these conditions. NMR time domain data were processed with the nmrPipe package[22] and the spectra were analyzed by using

Sparky software (T. D. Goddard and D. G. Kneller, University of California, San Francisco).

Acknowledgements

We thank K. Senda and K. Hattori (Nagoya City University) for help in the preparation of the recombinant proteins for NMR spectroscopy. We also thank M. Nakano (IMS) and T. Sugihara (JEOL) for help in NMR measurements and K. Matsumoto (RIKEN) for assistance in MS. We thank Drs. H. Sezaki, A. Hayashi, and T. Hosono (Agilent Technologies Japan) for their kind support in liquid chromatography–electrospray ionization MS analysis. This work was supported in part by Grants-in-Aid for Scientific Research on Priority Areas, Research on Pathomechanisms of Brain Disorders (to Y.Y., K.K., and M.H.), Grants-in-Aid for Scientific Research on Innovative Areas, Molecular Science of Fluctuations toward Biological Functions (to K.K.), and "Nanotechnology Network Project" of the Ministry of Education, Culture, Sports, Science and Technology (MEXT). This work was also supported by Takeda Science Foundation (Y.Y.).

Supplementary Data

Supplementary data associated with this article can be found, in the online version, at **doi:10.1016/j.jmb.2009.10.068**

References

1. Conway, K. A., Rochet, J. C., Bieganski, R. M. & Lansbury, P. T., Jr (2001). Kinetic stabilization of the α-synuclein protofibril by a dopamine-α-synuclein adduct. *Science*, **294**, 1346–1349.
2. Li, H. T., Lin, D. H., Luo, X. Y., Zhang, F., Ji, L. N., Du, H. N. *et al.* (2005). Inhibition of α-synuclein fibrillization by dopamine analogs via reaction with the amino groups of α-synuclein. Implication for dopaminergic neurodegeneration. *FEBS J.* **272**, 3661–3672.
3. Masuda, M., Suzuki, N., Taniguchi, S., Oikawa, T., Nonaka, T., Iwatsubo, T. *et al.* (2006). Small molecule inhibitors of α-synuclein filament assembly. *Biochemistry*, **45**, 6085–6094.
4. Porat, Y., Abramowitz, A. & Gazit, E. (2006). Inhibition of amyloid fibril formation by polyphenols: structural similarity and aromatic interactions as a common inhibition mechanism. *Chem. Biol. Drug Des.* **67**, 27–37.
5. Feng, B. Y., Toyama, B. H., Wille, H., Colby, D. W., Collins, S. R., May, B. C. *et al.* (2008). Small-molecule aggregates inhibit amyloid polymerization. *Nat. Chem. Biol.* **4**, 197–199.
6. Norris, E. H., Giasson, B. I., Hodara, R., Xu, S., Trojanowski, J. Q., Ischiropoulos, H. & Lee, V. M. (2005). Reversible inhibition of α-synuclein fibrillization by dopaminochrome-mediated conformational alterations. *J. Biol. Chem.* **280**, 21212–21219.
7. Herrera, F. E., Chesi, A., Paleologou, K. E., Schmid, A., Munoz, A., Vendruscolo, M. *et al.* (2008). Inhibition of α-synuclein fibrillization by dopamine is mediated by interactions with five C-terminal residues and with E83 in the NAC region. *PLoS ONE*, **e3394**, 3.
8. Ehrnhoefer, D. E., Bieschke, J., Boeddrich, A., Herbst, M., Masino, L., Lurz, R. *et al.* (2008). EGCG redirects amyloidogenic polypeptides into unstructured, off-pathway oligomers. *Nat. Struct. Mol. Biol.* **15**, 558–566.
9. Moussa, C. E., Mahmoodian, F., Tomita, Y. & Sidhu, A. (2008). Dopamine differentially induces aggregation of A53T mutant and wild type α-synuclein: insights into the protein chemistry of Parkinson's disease. *Biochem. Biophys. Res. Commun.* **365**, 833–839.
10. Rao, J. N., Dua, V. & Ulmer, T. S. (2008). Characterization of α-synuclein interactions with selected aggregation-inhibiting small molecules. *Biochemistry*, **47**, 4651–4656.
11. Hong, D. P., Fink, A. L. & Uversky, V. N. (2008). Structural characteristics of α-synuclein oligomers stabilized by the flavonoid baicalein. *J. Mol. Biol.* **383**, 214–223.
12. Masuda, M., Hasegawa, M., Nonaka, T., Oikawa, T., Yonetani, M., Yamaguchi, Y. *et al.* (2009). Inhibition of α-synuclein fibril assembly by small molecules: analysis using epitope-specific antibodies. *FEBS Lett.* **583**, 787–791.
13. Sasakawa, H., Sakata, E., Yamaguchi, Y., Masuda, M., Mori, T., Kurimoto, E. *et al.* (2007). Ultra-high field NMR studies of antibody binding and site-specific phosphorylation of α-synuclein. *Biochem. Biophys. Res. Commun.* **363**, 795–799.
14. Uversky, V. N., Yamin, G., Souillac, P. O., Goers, J., Glaser, C. B. & Fink, A. L. (2002). Methionine oxidation inhibits fibrillation of human α-synuclein *in vitro*. *FEBS Lett.* **517**, 239–244.
15. Paz, M. A., Gallop, P. M., Torrelio, B. M. & Fluckiger, R. (1988). The amplified detection of free and bound methoxatin (PQQ) with nitroblue tetrazolium redox reactions: insights into the PQQ-locus. *Biochem. Biophys. Res. Commun.* **154**, 1330–1337.
16. Ingrosso, D., Fowler, A. V., Bleibaum, J. & Clarke, S. (1989). Specificity of endoproteinase Asp-N (Pseudomonas fragi): cleavage at glutamyl residues in two proteins. *Biochem. Biophys. Res. Commun.* **162**, 1528–1534.
17. Tetaz, T., Morrison, J. R., Andreou, J. & Fidge, N. H. (1990). Relaxed specificity of endoproteinase Asp-N: this enzyme cleaves at peptide bonds N-terminal to glutamate as well as aspartate and cysteic acid residues. *Biochem. Int.* **22**, 561–566.
18. Stadtman, E. R., Van Remmen, H., Richardson, A., Wehr, N. B. & Levine, R. L. (2005). Methionine oxidation and aging. *Biochim. Biophys. Acta*, **1703**, 135–140.
19. Rospigliosi, C. C., McClendon, S., Schmid, A. W., Ramlall, T. F., Barre, P., Lashuel, H. A. & Eliezer, D. (2009). E46K Parkinson's-linked mutation enhances C-terminal-to-N-terminal contacts in α-synuclein. *J. Mol. Biol.* **388**, 1022–1032.
20. Jakes, R., Spillantini, M. G. & Goedert, M. (1994). Identification of two distinct synucleins from human brain. *FEBS Lett.* **345**, 27–32.
21. Masuda, M., Dohmae, N., Nonaka, T., Oikawa, T., Hisanaga, S., Goedert, M. & Hasegawa, M. (2006). Cysteine misincorporation in bacterially expressed human α-synuclein. *FEBS Lett.* **580**, 1775–1779.
22. Delaglio, F., Grzesiek, S., Vuister, G. W., Zhu, G., Pfeifer, J. & Bax, A. (1995). NMRPipe: a multidimensional spectral processing system based on UNIX pipes. *J. Biomol. NMR*, **6**, 277–293.

NEUROPATHOLOGY

Neuropathology 2010; **30**, 170–181 doi:10.1111/j.1440-1789.2009.01089.x

Symposium: Advances in amyotrophic lateral sclerosis research

Phosphorylated and cleaved TDP-43 in ALS, FTLD and other neurodegenerative disorders and in cellular models of TDP-43 proteinopathy

Tetsuaki Arai,[1] Masato Hasegawa,[2] Takashi Nonoka,[2] Fuyuki Kametani,[2] Makiko Yamashita,[2] Masato Hosokawa,[1] Kazuhiro Niizato,[1,3] Kuniaki Tsuchiya,[1,4] Zen Kobayashi,[1,5] Kenji Ikeda,[6] Mari Yoshida,[7] Mitsumoto Onaya,[8] Hiroshige Fujishiro[9] and Haruhiko Akiyama[1]

Departments of [1]Psychogeriatrics and [2]Molecular Neurobiology, Tokyo Institute of Psychiatry, Tokyo Metropolitan Organization for Medical Research, Departments of [3]Psychiatry and [4]Laboratory Medicine and Pathology, Tokyo Metropolitan Matsuzawa Hospital, [5]Department of Neurology and Neurological Science, Graduate School, Tokyo Medical and Dental University, Tokyo, [6]Zikei Hospital, Zikei Institute of Psychiatry, Okayama, [7]Department of Neuropathology, Institute for Medical Science of Aging, Aichi Medical University, Aichi, [8]Department of Neuropsychiatry, National Shimofusa Mental Hospital, Chiba, [9]Juntendo Tokyo Koto Geriatric Medical Center, Juntendo University School of Medicine, Tokyo, Japan

Transactivation response (TAR) DNA-binding protein of Mr 43 kDa (TDP-43) is a major component of the tau-negative and ubiquitin-positive inclusions that characterize amyotrophic lateral sclerosis (ALS) and frontotemporal lobar degeneration which is now referred to as FTLD-TDP. Concurrent TDP-43 pathology has been reported in a variety of other neurodegenerative disorders such as Alzheimer's disease, forming a group of TDP-43 proteinopathy. Accumulated TDP-43 is characterized by phosphorylation and fragmentation. There is a close relationship between the pathological subtypes of FTLD-TDP and the immunoblot pattern of the C-terminal fragments of phosphorylated TDP-43. These results suggest that proteolytic processing of accumulated TDP-43 may play an important role for the pathological process. In cultured cells, transfected C-terminal fragments of TDP-43 are more prone to form aggregates than full-length TDP-43. Transfecting the C-terminal fragment of TDP-43 harboring pathogenic mutations of TDP-43 gene identified in familial and sporadic ALS cases into cells enhanced the aggregate formation. Furthermore, we found that methylene blue and dimebon inhibit aggregation of TDP-43 in these cellular models. Understanding the mechanism of phosphorylation and truncation of TDP-43 and aggregate formation may be crucial for clarifying the pathogenesis of TDP-43 proteinopathy and for developing useful therapeutics.

Key words: α-synuclein, fragment, inclusion, phosphorylation, tau.

INTRODUCTION

Transactivation response (TAR) DNA-binding protein of Mr 43 kDa (TDP-43) is a major component of the tau-negative and ubiquitin-positive inclusions that characterize amyotrophic lateral sclerosis (ALS) and the most common pathological subtype of frontotemporal lobar degeneration (FTLD-U), which is now referred to as FTLD-TDP.[1–7] Several genes and chromosomal loci, including the progranulin gene (*PGRN*),[8,9] valosin-containing protein gene (*VCP*)[10] and an unidentified gene at chromosome 9p,[11,12] have been reported to be associated with familial forms of FTLD-TDP. Recent findings of various missense mutations of TDP-43 gene (*TARDBP*) in familial and sporadic ALS cases prove the essential role of abnormal TDP-43 in neurodegeneration.[13–17] These disorders are now collectively referred to as TDP-43 proteinopathy.[1–4]

Correspondence: Haruhiko Akiyama, MD, PhD, Departments of Psychogeriatrics, Tokyo Institute of Psychiatry, Tokyo Metropolitan Organization for Medical Research, 2-1-8 Kamikitazawa, Setagaya-ku, Tokyo 156-8585, Japan. Email: akiyama@prit.go.jp

Received 29 October 2009; revised 14 November 2009 and accepted 15 November 2009; published online 19 January 2010.

TDP-43 was first isolated as a transcriptional inactivator binding to the TAR DNA element of the HIV-1 virus.[18] It appears to belong to the group of 2 RNA-binding domain (RBD)-Gly RNA-binding proteins, which include the heterogeneous nuclear ribonucleoprotein (hnRNP) family and factors involved in RNA splicing and transport.[19] Subsequent studies reported that TDP-43 functions to inhibit expression of mouse spermatid-specific SP-10 gene and of cyclin-dependent kinase 6, to regulate alternative splicing of exon 9 of cystic fibrosis transmembrane conductase regulator (*CFTR*), exon 3 of apolipoprotein A-II (*Apo AII*), and exon 7 of survival of motor neuron 2 (*SMN2*), and to stabilize human low molecular weight neurofilament (hNFL) mRNA.[20-26] The splicing inhibitory activity requires the C-terminal region of TDP-43 by interaction with other hnRNP members.[27] Furthermore, more recent studies suggest that TDP-43 may be involved in other cellular processes such as microRNA biogenesis, apoptosis, and cell division.[28]

Ubiquitin- and TDP-43-positive pathological inclusions found in FTLD-TDP include neuronal cytoplasmic inclusions (NCIs), dystrophic neurites (DNs), neuronal intranuclear inclusions (NIIs), and glial cytoplasmic inclusions (GCIs).[1,2,29-31] Based on morphological aspects, TDP-43 proteinopathies have been classified into four subtypes.[32] Type 1 is characterized by DNs with few NCIs and no NIIs, Type 2 has numerous NCIs with few DNs and no NIIs, Type 3 has numerous NCIs and DNs and an occasional NIIs and Type 4 has numerous NIIs and DNs with few NCIs. Type 4 is specific for familial FTLD-TDP with mutations of VCP gene. The strong relationship between other subtypes of TDP-43 pathology and clinical phenotype is indicated. Type 1 is associated with semantic dementia, Type 2 with FTLD with motor neuron disease (MND) or clinical signs of MND, and Type 3 with progressive non-fluent aphasia.[29,33,34]

In ALS, motoneuronal skein-like inclusions immunopositive for ubiquitin had been regarded as major pathological hallmarks. Recent detailed immunohistochemical studies have clarified the wide distribution of neuronal and glial TDP-43 pathology in multiple areas of the central nervous systems, including the nigro-striatal system, the neocortical and allocortical areas, and the cerebellum.[35,36] These findings suggest that ALS does not selectively affect only the motor system, but rather is a multisystem neurodegenerative TDP-43 proteinopathy affecting both neurons and glial cells.[35,36]

Biochemical analyses of the detergent-insoluble fraction extracted from brains of patients afflicted with FTLD-TDP and ALS show that TDP-43 accumulated in these pathological structures is phosphorylated and cleaved.[1,2]

In the present review, we will focus on the histological and biochemical abnormality of TDP-43 accumulated in ALS, FTLD-TDP and other neurodegenerative disorders, and on the establishment and analyses of cellular models for intracellular aggregates of TDP-43. Using antibodies specific for phosphorylated TDP-43 (pTDP-43), we identified several phosphorylation sites in the C-terminal region of the TDP-43 that accumulates in FTLD-TDP and ALS brains.[37] Furthermore, we found a close relationship between the pathological subtypes of FTLD-TDP and ALS and the immunoblot pattern of phosphorylated C-terminal fragments of TDP-43, suggesting that proteolytic processing may be crucial in the pathological process of these diseases.[37] By transfecting deletion mutants lacking nuclear localization signal or C-terminal fragments of TDP-43, we succeeded in establishing the cellular models of TDP-43 proteinopathy. By analyzing them, we found the pathogenic effect of mutations of TDP-43 gene identified in ALS cases, and the potential therapeutic agents that inhibit the aggregate formation of TDP-43.

IMMUNOHISTOCHEMICAL AND BIOCHEMICAL ANALYSIS FOR PTDP-43 IN ALS AND FTLD-TDP

In order to identify the critical phosphorylation sites of TDP-43, we raised antibodies against 39 different synthetic phosphopeptides, representing 36 out of 63 candidate phosphorylation sites.[37] Of the generated antibodies, pS379, pS403/404, pS409, pS410 and pS409/410 stained the inclusions in immunohistochemistry, and abnormal TDP-43 species on immunoblot, in FTLD-TDP and ALS cases. Since the immunoreactivity of pS409/410 was particularly robust in both immunohistochemistry and immunoblotting, we later produced a monoclonal antibody directed against phosphoserines 409 and 410 in human TDP-43.[38] The results suggest that at least five sites on TDP-43 are phosphorylated in subjects with FTLD-TDP and ALS, and that abnormal phosphorylation takes place mainly near the carboxyl (C)-terminal region of TDP-43.

In immunohistochemistry, in contrast to the commercially obtained phosphorylation-independent anti-TDP-43 antibody, which labels both abnormal structures and normal nuclei (Fig. 1A), pTDP-43-specific antibodies recognized only abnormal structures, including NCIs (Fig. 1B), NIIs (Fig. 1B, inset), DNs (Fig. 1C), round inclusions (Fig. 1D), skein-like inclusions (Fig. 1E), and GCIs (Fig. 1F). In double immunofluorescence staining for pTDP-43 (Fig. 1G, red) and a complement protein, C4d (Fig. 1H, green), pTDP-43-positive inclusions were often found in C4d-positive oligodendrocytes (Fig. 1I), indicating that most GCIs are oligodendrocytic in origin. In the frontal cortex of the ALS case with a long duration, we

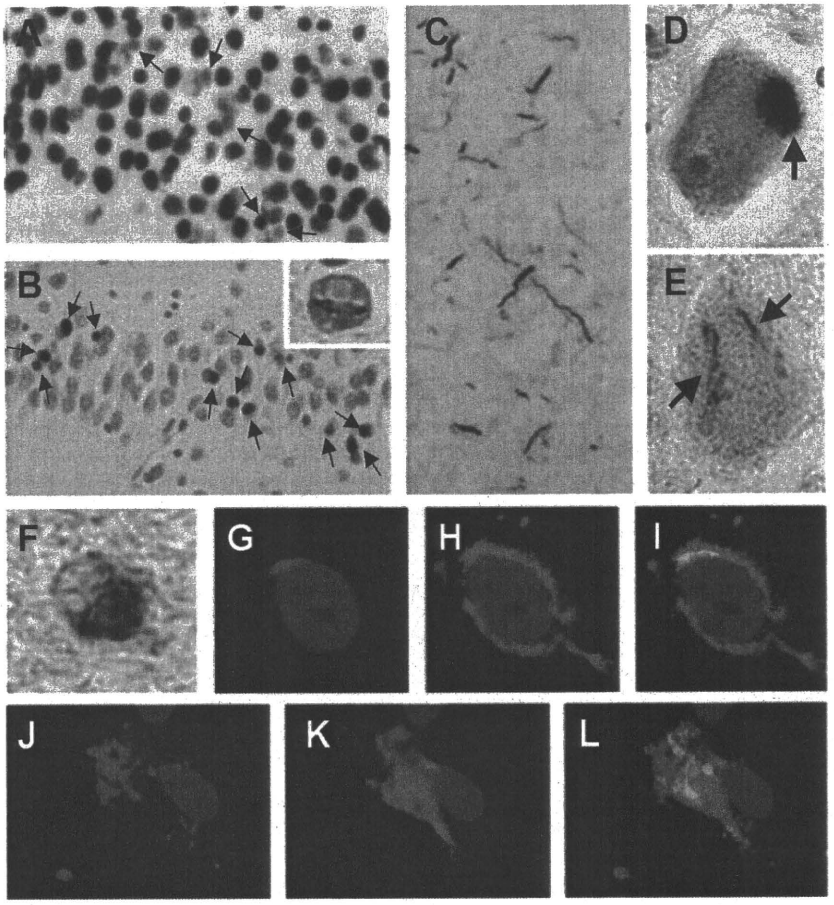

Fig. 1 Neuronal and glial inclusions immunopositive for phosphorylated transactivation response (TAR) DNA-binding protein of Mr 43 kDa (TDP-43) in frontotemporal lobar degeneration (FTLD)-TDP and ALS. A. Dentate gyrus (DG) of the hippocampus of the FTLD-TDP case stained with the commercially available phosphorylation-independent anti-TDP-43 antibody. Both neuronal cytoplasmic inclusions (NCIs) (arrows) and normal neuronal nuclei are immunopositive. B. Dentate gyrus of the FTLD-TDP case stained with the pTDP-43-specific antibody (pS409/410). NCIs are clearly stained with no nuclear staining. Inset represents neuronal intranuclear inclusions with a cat-eye shape. C. Dystrophic neurites in the temporal cortex of the FTLD-TDP positive for pS409/410. Motoneuronal round inclusion (D) and skein-like inclusion (E) of the ALS case are stained with pS409/410. F. Glial cytoplasmic inclusions in the motor system of the ALS case stained with pS409/410. In double-label immunofluorescence histochemistry using pS409/410 (red in G, I) and anti-C4d (green in H, I), the pS409/410-positive inclusion (red) is present around the nucleus of the C4d-positive oligodendrocyte (green) (I). In the frontal cortex of the ALS case with long duration, double-label immunofluorescence using pS409/410 (red in J, L) and anti-GFAP (green in K, L) shows a partial colocalization of the both proteins in the cytoplasm of the astrocyte.

found a partial colocalization of pTDP-43 and GFAP in the cytoplasm of astrocytes (Fig. 1J–L). These results suggest that all of the inclusion types previously described in FTLD-TDP and ALS contain pTDP-43.

Immunoblot analyses of sarkosyl-insoluble fractions with pTDP-43-specific antibodies revealed a single band at 45 kDa, several smaller fragments at ~25 kDa and indistinct smears in FTLD-TDP and ALS cases but not in controls (Fig. 2A). The intensity of the ~25 kDa fragments tended to be greater than that of the 45 kDa band in FTLD-TDP and in ALS. All of the immunoreactive bands were completely abolished by lambda protein phosphatase treatment, proving the specificity of the antibodies to the phosphoepitopes.

To investigate the biochemical basis of the different TDP-43 pathological subtypes (Types 1–3), we carefully compared the results of immunoblots of the sarkosyl-insoluble fractions from the cerebral cortex of cases with sporadic FTLD-TDP (Type 1), FTLD-MND (Type 2), ALS (Type 2) and familial FTLD with *PGRN* mutations (m*PGRN*) (Type 3), using pTDP-43 specific antibodies. The results showed that there is a close relationship between the pathological subtypes and the immunoblot pattern of the 18–26 kDa C-terminal fragments of pTDP-43 (Fig. 2B,C). These findings confirm and extend the previous reports[1,31] that showed C-terminal fragment composition varied between cases with Type 1 and Type 2 pathology. Furthermore, these results parallel our earlier findings of differing C-terminal tau fragments in progressive supranuclear palsy and corticobasal degeneration, despite identical composition of tau isoforms.[39] Taken together, these results suggest that elucidating the mechanism of C-terminal fragment origination may shed light on the pathogenesis of several neurodegenerative disorders involving TDP-43 proteinopathy and tauopathy.

TDP-43-POSITIVE STRUCTURES IN A VARIETY OF NEURODEGENERATIVE DISORDERS AND THE SUBCLASSIFICATION OF TDP-43 PROTEINOPATHY

Immunohistochemical examination, using commercially available phosphorylation-independent anti-TDP-43 antibodies, had demonstrated abnormal intracellular accumulation of TDP-43 in neurodegenerative disorders other

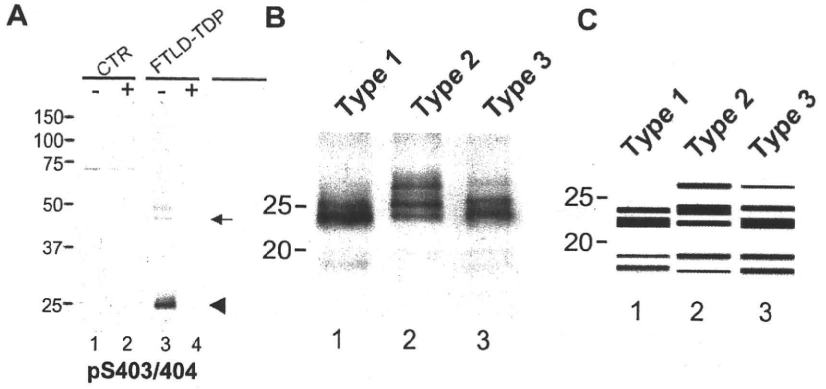

Fig. 2 Biochemical analyses using antibodies specific for phosphorylated transactivation response (TAR) DNA-binding protein of Mr 43 kDa (pTDP-43). A. Immunoblot analyses of sarkosyl-insoluble fractions from control (lanes 1, 2) and frontotemporal lobar degeneration (FTLD)-TDP (lanes 3, 4), using pS403/404, before (–) and after (+) the treatment with lambda protein phosphatase. pS403/404 specifically label the ~45 kDa band (arrow) and the ~25 kDa fragments (arrowhead) as well as a smear, only in FTLD-TDP (lane 3). These immunoreactivities are abolished after dephosphorylation. B. Representative immunoblots with the pTDP-43 specific antibody, pS409/410. The sporadic FTLD-TDP case with Type 1 pathology shows two major bands at 23 and 24 kDa and two minor bands at 18 and 19 kDa (lane 1), while the FTLD-MND (motor neurone disease) case with Type 2 pathology shows three major bands at 23, 24 and 26 kDa and two minor bands at 18 and 19 kDa (lane 2). A 23 kDa band is the most intense in sporadic FTLD-TDP (lane 1), while a 24 kDa band is the most intense in FTLD-MND (lane 2). The band pattern of the case of familial FTLD with progranulin gene mutations with Type 3 pathology is not distinctive but intermediate between FTLD-TDP and FTLD-MND (lane 3). C. Schematic diagram showing the band pattern of the C-terminal fragments of pTDP-43.

than FTLD-TDP and ALS, including ALS/parkinsonism-dementia complex of Guam,[40–42] Alzheimer's disease (AD),[43–47] dementia with Lewy bodies (DLB),[44,48] Pick's disease,[2,49,50] hippocampal sclerosis,[43] and corticobasal degeneration (CBD).[47] However, the biochemical features of accumulated TDP-43, especially its phosphorylation sites and fragmentation, had been unclear in these disorders. To address these issues, we performed immunohistochemical and biochemical analyses of TDP-43 in cases of neurodegenerative disorders, using our pTDP-43-specific antibodies. As a result, we found a high frequency of pTDP-43 pathology in cases of AD (36–56%) (Fig. 3A,C), DLB (53–60%) (Fig. 3B,D), argyrophilic grain disease (AGD) (60%) (Fig. 3E), Huntington's disease (100%), and a case of familial British dementia.[51–54]

The pathological significance and mechanism of such a frequent co-occurrence of diverse protein aggregates are still unclear. A higher Braak NFT stage in the TDP-43-positive patients than in the TDP-43-negative ones was found in DLB+AD cases by Nakashima-Yasuda *et al.*[48] and in our study of AD cases.[51] We also reported parallel distribution of TDP-43-positive structures and tau-positive grains and higher AGD stages in cases with TDP-43 immunoreactivity than in those without TDP-43 immunoreactivity in AGD.[53] Double-label immunofluorescence microscopy reveals partial colocalization of tau and TDP-43 in AD, DLB, AGD, Guamanian PDC and CBD[40,41,43,44,47,48,53] or of α-synuclein and TDP-43 in DLB.[44,48,51] These findings suggest that there may be common factors or mechanisms that affect the conformation or modification of both proteins, leading to their intracellular accumulation. Nakashima-Yasuda *et al.* indicated two possibilities of the basis for those.[48] One is the direct interaction between the protein as tau and α-synuclein promote the fibrillization of each other *in vitro*.[55] The other is that the misfolding and aggregation of a disease protein disrupt normal cellular functions, leading to predisposing other proteins to aggregate.

Table 1 Subclassification of TDP-43 proteinopathy

1. pure TDP-43 proteinopathy	
Disease	Gene (locus)
A. Familial	
FTDU-17 (FTLD-TDP, Type 3)	PGRN
IBMPFD (FTLD-TDP, Type 4)	VCP
Perry syndrome	DCTN1
ALS	TARDBP (TDP-43)
FTLD-MND (FTLD-TDP, Type 2)	Chromosome 9
B. Sporadic	
FTLD-TDP (Types 1-3)	
ALS	
2. Combined TDP-43 proteinopathy	
Disease	Aggregated proteins
A. Familial	
FBD	ABri, Tau, TDP-43
HD	Huntingtin, TDP-43
MJD (SCA3)	Ataxin-3, TDP-43
B. Sporadic	
AD	Tau, TDP-43
DLB	Tau, Alpha-syn, TDP-43
CBD	Tau, TDP-43
AGD	Tau, TDP-43
C. Endemic	
Guam ALS/PDC	Tau, Alpha-syn, TDP-43
Kii ALS/PDC	Tau, Alpha-syn, TDP-43

FTDU-17, frontotemporal dementia with ubiquitinated inclusions linked to chromosome 17; PGRN, progranulin; IMBPFD, inclusion body myopathy associated with Paget disease of bone and frontotemporal dementia; DCTN1, dynactin 1; ALS, amyotrophic lateral sclerosis; TARDBP (TDP-43), TAR DNA-binding protein of 43 kDa.

AD, Alzheimer's disease; AGD, argyrophilic grain disease; Alpha-syn, α-synuclein; CBD, corticobasal degeneration; DLB, dementia with Lewy bodies; FBD, familial British dementia; FTLD-MND, frontotemporal lobar degeneration with motor neuron disease; HD, Huntington disease; MJD, Machado-Joseph disease; PDC, parkinsonism-dementia complex; SCA, Spinocerebellar ataxia.

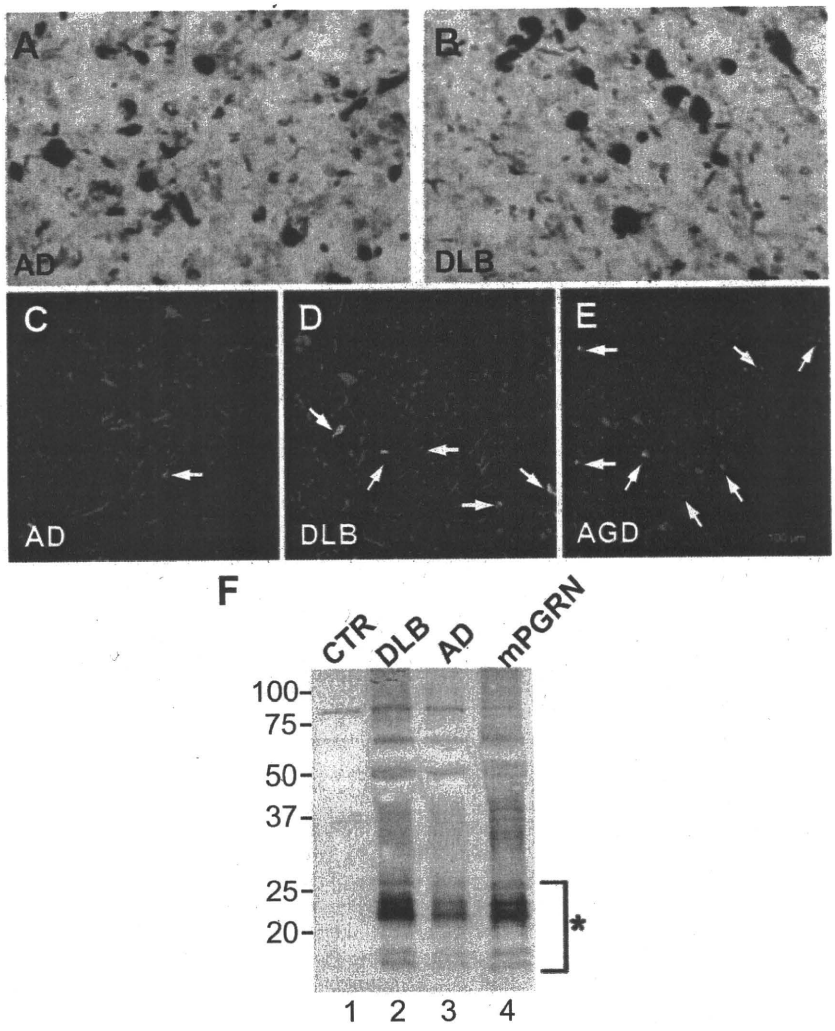

Fig. 3 Phosphorylated transactivation response (TAR) DNA-binding protein of Mr 43 kDa (pTDP-43)-positive structures in other neurodegenerative disorders. A. Neuronal cytoplasmic inclusions (NCIs) and dystrophic neurites stained with the pTDP-43-specific antibody (pS403/404) in the temporal cortex of the Alzheimer's disease (AD) case (A) and the dementia with Lewy bodies (DLB) case (B) with diffuse TDP-43 pathology. (C–E) Double-label immunofluorescence histochemistry of the temporal cortex of AD (**C**) and DLB (D) and of the amygdala of argyrophilic grain disease (AGD) (E). The green fluorescence reveals the immunoreactivity for phosphorylated tau (AT8) in C and E, and that for phosphorylated α-synuclein in D, while the red fluorescence represents the immunopositivity for pS403/404 in C–E. Arrows indicate the colocalization of tau and pTDP-43 in C and E, and that of α-synuclein and pTDP-43 in D. F. The band pattern of the C-terminal fragments of pTDP-43 (asterisk) in DLB (lane 2) and AD (lane 3) is similar to that in familial FTLD with progranulin gene mutation (mPGRN).

Of the TDP-43-positive cases in AD and DLB, about 20–30% showed neocortical TDP-43 pathology resembling the FTLD-TDP, Type 3[51] (Fig. 3A,B). Immunoblot analyses of the sarkosyl-insoluble fraction from cases with neocortical TDP-43 pathology showed intense staining of several low-molecular-weight bands, corresponding to C-terminal fragments of TDP-43. Interestingly, the band pattern of these C-terminal fragments in AD and DLB also corresponds to that previously observed in the FTLD-TDP, Type 3[37] (Fig. 3F). These results suggest that the morphological and biochemical features of TDP-43 pathology are common between AD or DLB and a specific subtype of FTLD-TDP. Since all FTLD-TDP cases with PGRN mutations show Type 3 pathology,[56] there may be genetic factors, such as mutations or genetic variants of *PGRN* underlying the co-occurrence of abnormal deposition of TDP-43, tau and α-synuclein.

The clinical impact of the concurrent TDP-43 pathology in other neurodegenerative disorders than FTLD-TDP and ALS is also not fully understood. Uryu *et al.* reported a lack of association between TDP-43 pathology and clinical manifestation of AD.[47] Similarly, we did not find a significant difference of clinical features between AGD cases with and without TDP-43 pathology.[53] Joseph *et al.* on the other hand, reported that AD cases with TDP-43 pathology were older at onset and death, and performed worse on the Clinical Dementia Rating Scale, Mini-Mental State Examination, and Boston Naming Test than those without TDP-43 pathology.[46] The older age at death of the AD cases with TDP-43 pathology was also observed in our study.[51] Nakashima-Yasuda *et al.* found a higher average age at death in the TDP-43 positive cases in Lewy body-related diseases with dementia.[48] Further studies using larger cohorts with more detailed clinical, radiological and pathological data are needed to elucidate the clinical impact of TDP-43 pathology in a variety of neurodegenerative disorders.

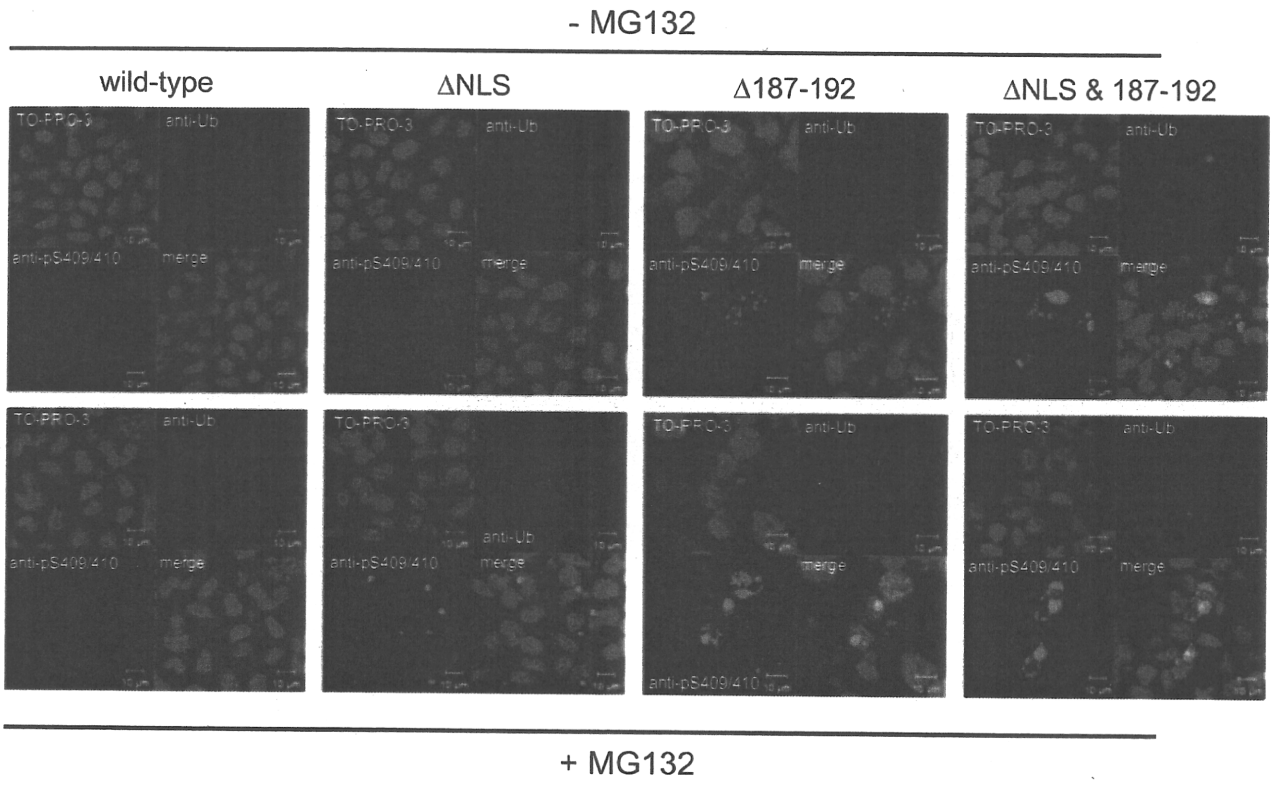

Fig. 4 The formation of inclusion-like structures in cells transfected with deletion mutants of transactivation response (TAR) DNA-binding protein of Mr 43 kDa (TDP-43). When pcDNA3-TDP-43 wild-type was expressed in SH-SY5Y cells, no staining was observed by the phosphorylation-specific anti-TDP-43 antibody (pS409/410), indicating that transfected wild-type TDP-43 and endogenous TDP-43 are not phosphorylated at Ser409/410. The deletion mutant lacking nuclear localization signal (ΔNLS: 78–84 residues) was not recognized by pS409/410 without MG132 treatment, while round cytoplasmic inclusion-like structures were stained by both pS409/410 and anti-ubiquitin antibodies in those cells treated with MG132. In cells expressing another deletion mutant lacking 187–192 residues (Δ187–192), pS409/410-positive but ubiquitin-negative intranuclear dot-like structures were observed without treatment. With MG132, round intranuclear inclusions positive for pS409/410 and ubiquitin were formed. In cells expressing the double-deletion mutant (ΔNLS and 187–192), cytoplasmic inclusions positive for pS409/410 and ubiquitin were formed even in the absence of MG132.

Based on these findings so far, we would like to propose that TDP-43 proteinopathy can be divided into two groups (Table 1). One is "pure" TDP-43 proteinopathy, in which only TDP-43 accumulates in brains as a pathological protein. The other is "combined" TDP-43 proteinopathy, which shows multiple protein aggregates. TDP-43 pathology is always found in all cases of pure TDP-43 proteinopathy and familial and endemic cases of combined TDP-43 proteinopathy, while it is found in a subpopulation of cases with sporadic combined TDP-43 proteinopathy.

ESTABLISHMENT AND ANALYSES OF CELLULAR MODELS OF TDP-43 PROTEINOPATHY

To establish the cellular models for intracellular aggregates of TDP-43, we first examined two candidate sequences for the nuclear localization signal (NLS) (Fig. 4).[57] Deletion of residues 78–84 resulted in cytoplasmic localization of TDP-43 in SH-SY5Y cells, proving that this sequence indeed functions as NLS. This result is largely consistent with the previous report by Winton *et al.* which showed that residues 82–98 were required for TDP-43 entry into the nucleus.[58] On the other hand, the mutant lacking residues 187–192 localized in nuclei, forming unique dot-like structures. Proteasome inhibition caused these to assemble into aggregates. Furthermore, double-deletion mutant of these sequences caused cytoplasmic inclusion formation without proteasomal inhibition. Immunohistochemical and immunoblot analyses showed that these inclusions consisted of phosphorylated and ubiquitinated TDP-43, suggesting that these cellular models recapitulate the phenotypes of TDP-43 proteinopathies both pathologically and biochemically.

Then, we tried to generate and analyze the cellular models by expressing C-terminal fragments of TDP-43 in

SH-SY5Y cells, since 18–26 kDa C-terminal fragments of TDP-43 are major constituents of inclusions in FTLD-TDP and ALS brains.[37] The results showed that expression of several TDP-43 C-terminal fragments as green fluorescent protein (GFP), including 162–414, 218–414, 219–414 and 247–414, led to the formation of cytoplasmic inclusions positive for pTDP-43 and ubiquitin (Fig. 5).[59] The N-termini of the latter two peptides, 219–414 and 247–414, correspond to the cleavage sites of TDP-43 C-terminal fragments accumulated in FTLD-TDP brains identified by our mass spectra analyses. Igaz *et al.* reported another cleavage site at Arg 208 in a pathological TDP-43 C-terminal fragment from FTLD-TDP brains and inclusion formation in cultured cells expressing resultant C-terminal fragment (residues 208–414).[60] Our immunoblot analysis showed that these aggregated pTDP-43 C-terminal fragments were recovered in sarkosyl-insoluble fraction as those in brains of FTLD-TDP and ALS.

Several groups have recently reported increased accumulation of TDP-43 fragments in the brain homogenates[13] and cultured cells[15,16] in some of the pathogenic mutations of TARDBP identified in ALS. However, in our cellular models, immunoblot analyses failed to show any significant differences in the generation of fragments of TDP-43 with or without various mutations. Alternatively, pathogenic mutations consistently enhanced aggregation of TDP-43 if they are present in the C-terminal fragment, GFP-TDP 162–414 (Fig. 6). These results suggest that pathogenic mutations and N-terminal truncation synergistically promote abnormal accumulation of TDP-43.

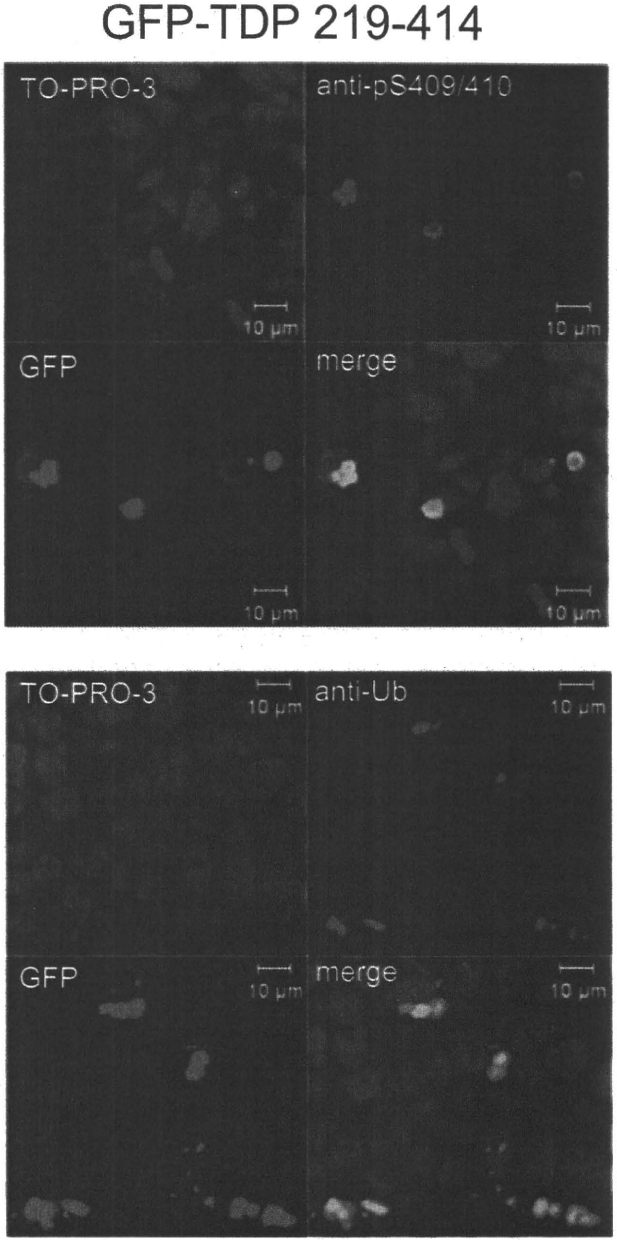

Fig. 5 Transactivation response (TAR) DNA-binding protein of Mr 43 kDa (TDP-43) C-terminal fragments identified in diseased brains form cytoplasmic inclusions in cells. Round cytoplasmic inclusions with strong green fluorescent protein (GFP) intensities were observed in SH-SY5Y cells expressing GFP-TDP 219–414. These were positive for pS409/410 and ubiquitin Ub).

METHYLENE BLUE AND DIMEBON INHIBIT AGGREGATION OF TDP-43 IN CELLULAR MODELS

Inhibition of the aggregation of TDP-43 and promotion of its clearance are considered to be major therapeutic avenues for ALS and FTLD-TDP. As for other neurodegenerative diseases, current tools include antibodies, synthetic peptides, molecular chaperones and chemical compounds. Of the latter, methylene blue (MB) and dimebon have recently been reported to have significant beneficial effects in phase II clinical trials of AD.[61,62] MB is a phenothiazine compound that has been used for treating methemoglobinemia,[63,64] inhibiting nitric oxide synthase,[65] reducing nGMP,[66] enhancing β-oxidation in mitochondria,[67] inhibiting of noradrenalin re-uptake[68] and enhancing brain mitochondrial cytochrome oxidase activity.[69,70] It has also been shown to inhibit AD-like Aβ and tau aggregation *in vitro*.[71,72] Dimebon is a non-selective antihistaminergic compound that was in clinical use for many years before more selective agents became available.[73] It has been reported to inhibit butyrylcholinesterase, acetylcholinesterase, NMDA receptors, voltage-gated calcium channels, adrenergic receptors, histamine H1 receptors, histamine H2 receptors and serotonin receptors, as well as to stabilize glutamate-induced Ca2+ signals.[74–76] The effects of dimebon on pathological protein aggregation have not been studied in detail.

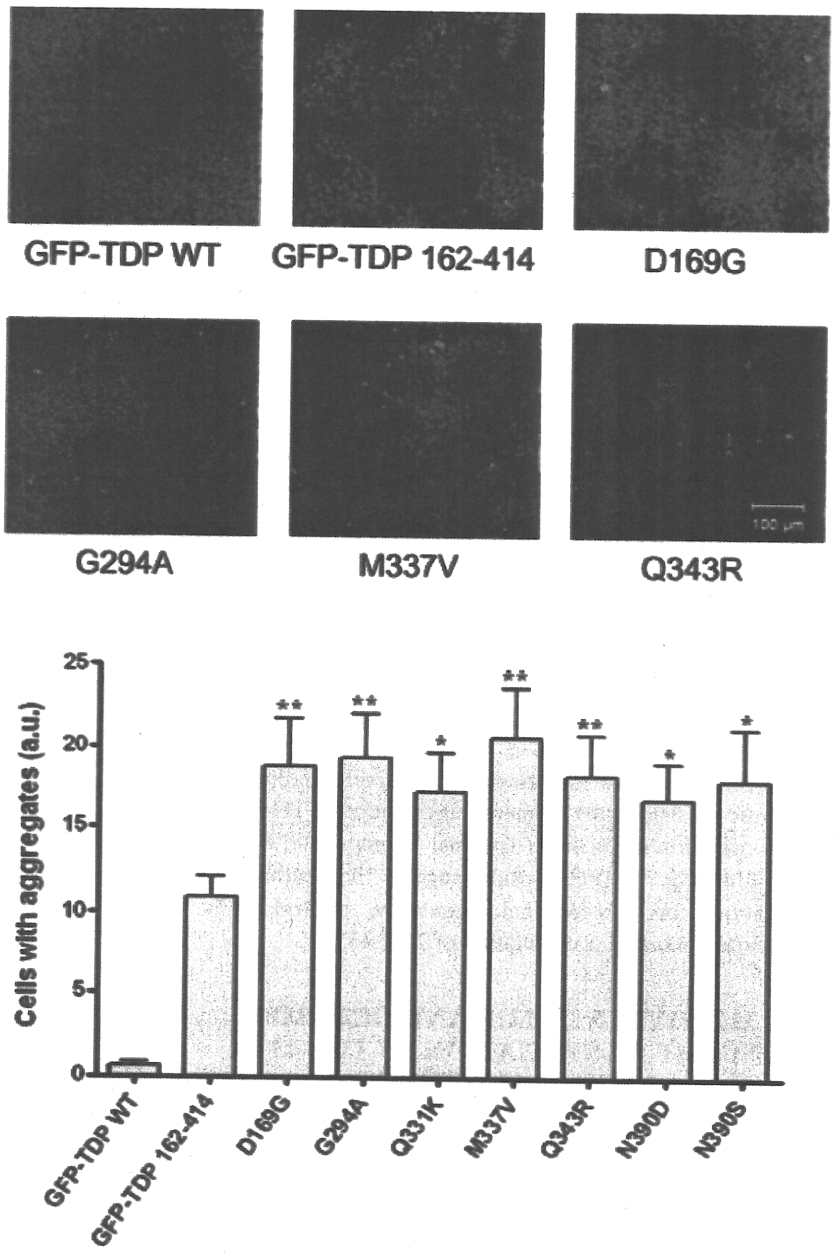

Fig. 6 The effect of transactivation response (TAR) DNA-binding protein of Mr 43 kDa (TDP-43) mutations on aggregates formation of the C-terminal fragment of TDP-43. All seven mutations significantly facilitated the formation of intracellular aggregates of green fluorescent protein (GFP)-TDP 162–414, as compared with those of wild-type GFP-TDP 162–414.

Using our cellular models of TDP-43 proteinopathy described above, we investigated the effects of MB and dimebon on the formation of TDP-43 aggregates.[77] Following treatment with 0.05 μM MB or 5 μM dimebon, the number of TDP-43 aggregates was reduced by 50% and 45%, respectively (Fig. 7A–C,I). The combined use of MB and dimebon resulted in an 80% reduction in the number of aggregates (Fig. 7D,I), and in the significant reduction of phosphorylated TDP-43 in insoluble fraction of the cell lysate (Fig. 7E–H). These results suggest that MB and dimebon may be useful for the treatment of ALS, FTLD-TDP and other TDP-43 proteinopathies.

CONCLUSION

Intracellular aggregation of TDP-43 takes place in brains of patients with ALS, FTLD and a variety of other neurodegenerative diseases, suggesting the possibility that TDP-43 has wide influence on neuronal dysfunction and neurodegeneration. Phosphorylated and truncated forms of TDP-43 are major species accumulated in diseased brains, and the proteolytic cleavage of TDP-43 may play an important role for the pathological process of TDP-43 proteinopathy. In cultured cells, expression of the TDP-43 C-terminal fragments results in accelerated aggregate formation and in

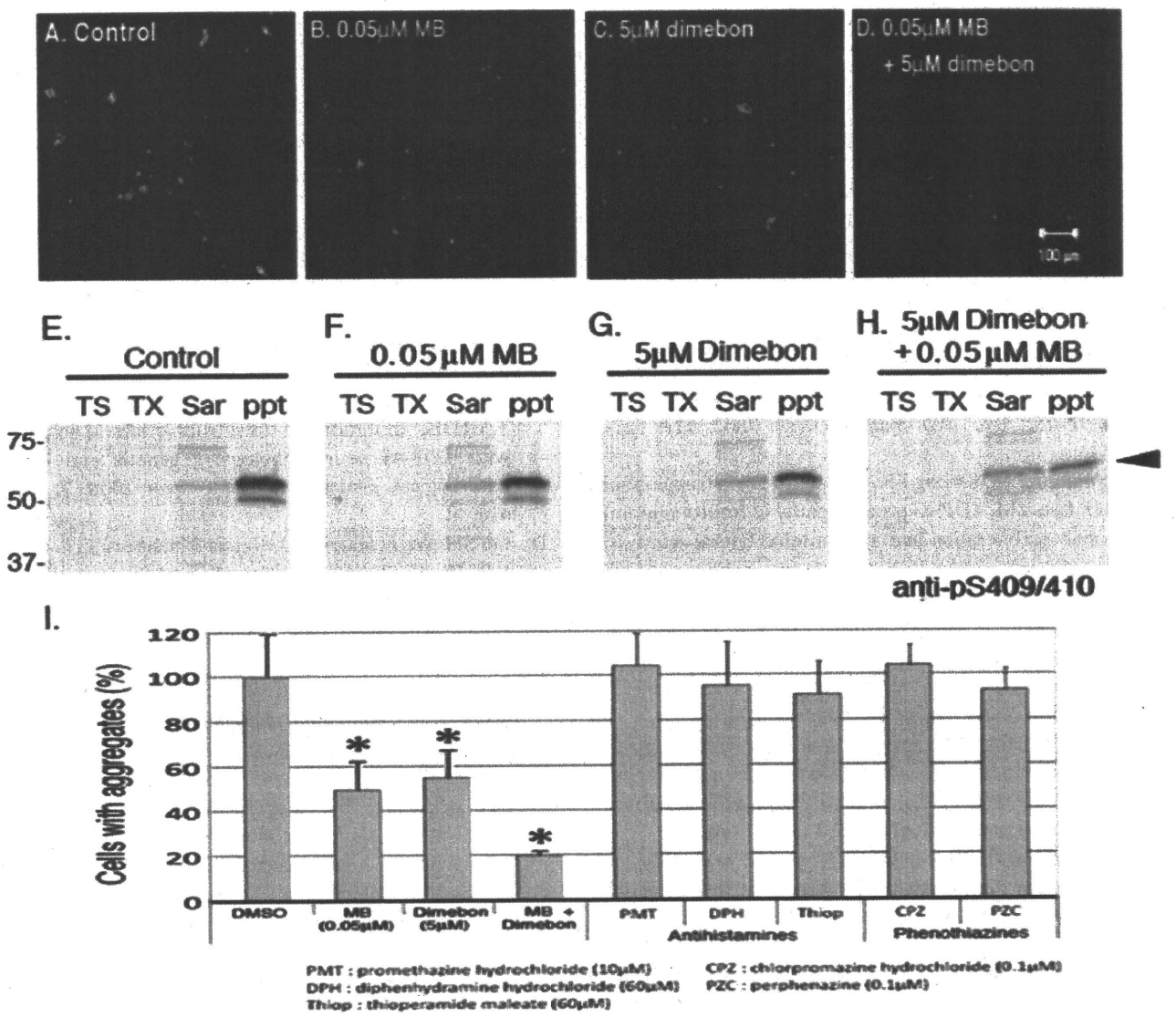

Fig. 7 Inhibition of aggregates formation of transactivation response (TAR) DNA-binding protein of Mr 43 kDa (TDP-43) in cellular models by methylene blue (MB) and dimebon. (A–D) Immunohistochemical analysis of the effects of MB and dimebon on the aggregation of TDP-43 in SH-SY5Y cells expressing TDP-43 (ΔNLS and 187–192). TDP-43 inclusions were stained with anti-pS409/410 antibody and detected with Alexa Fluor 488-labeled secondary antibody. Representative confocal images from cells treated with control (dimethyl sulfoxide + distilled water) (A), 0.05 μM MB (B), 5 μM dimebon (C) and 0.05 μM MB + 5 μM dimebon (D) are shown. (E–H): Immunoblot analysis of the effects of MB and dimebon on the aggregation of TDP-43 in SH-SY5Y cells expressing green fluorescent protein (GFP)-tagged TDP-43 C-terminal fragment (162–414). Tris saline (TS)-soluble material, Triton X-100 (TX)-soluble material, Sarkosyl (Sar)-soluble material and the remaining pellet (ppt) were prepared from control cells (E) and from cells treated with 0.05 μM MB (F), 5 μM dimebon (G), and 0.05 μM MB + 5 μM dimebon (H), run on SDS-PAGE and immunoblotted with anti-pS409/410 antibody. (I) Quantitation of cells with TDP-43 aggregates. The number of cells with intracellular TDP-43 aggregates was counted and expressed as the percentage of cells with aggregates in the absence of compound (taken as 100%). Data are means ± SEM $^*P < 0.01$ by Student's *t*-test.

failure of nuclear localization of endogenous TDP-43. At present, it is unknown whether loss of function, toxic gain of function, or a combination of both mechanisms contributes to neurodegeneration. Cultured cells or animal models expressing those abnormal TDP-43 species are expected to be useful tools to investigate the pathogenesis of TDP-43 proteinopathy and to develop effective diagnostics and therapeutics.

REFERENCES

1. Neumann M, Sampathu DM, Kwong LK *et al.* Ubiquitinated TDP-43 in frontotemporal lobar degeneration and amyotrophic lateral sclerosis. *Science* 2006; **314**: 130–133.
2. Arai T, Hasegawa M, Akiyama H *et al.* TDP-43 is a component of ubiquitin-positive tau-negative inclusions in frontotemporal lobar degeneration and amyotrophic lateral sclerosis. *Biochem Biophys Res Commun* 2006; **351**: 602–611.
3. Davidson Y, Kelley T, Mackenzie IRA *et al.* Ubiquitinated pathological lesions in frontotemporal lobar degeneration contain the TAR DNA-binding protein, TDP-43. *Acta Neuropathol (Berl)* 2007; **113**: 521–533.
4. Neumann M, Kwong LK, Sampathu DM, Trojanowski JQ, Lee VM. TDP-43 proteinopathy in frontotemporal lobar degeneration and amyotrophic lateral sclerosis: protein misfolding diseases without amyloidosis. *Arch Neurol* 2007; **64**: 1388–1394.
5. Mackenzie IR, Bigio EH, Ince PG *et al.* Pathological TDP-43 distinguishes sporadic amyotrophic lateral sclerosis from amyotrophic lateral sclerosis with SOD1 mutations. *Ann Neurol* 2007; **61**: 427–434.
6. Tan CF, Eguchi H, Tagawa A *et al.* TDP-43 immunoreactivity in neuronal inclusions in familial amyotrophic lateral sclerosis with or without SOD1 gene mutation. *Acta Neuropathol (Berl)* 2007; **113**: 535–542.
7. Mackenzie IR, Neumann M, Bigio EH *et al.* Nomenclature for neuropathologic subtypes of frontotemporal lobar degeneration: consensus recommendations. *Acta Neuropathol* 2009; **117**: 15–18.
8. Baker M, Mackenzie IR, Pickering-Brown SM *et al.* Mutations in progranulin cause tau-negative frontotemporal dementia linked to chromosome 17. *Nature* 2006; **442**: 916–919.
9. Cruts M, Gijselinck I, van der Zee J *et al.* Null mutations in progranulin cause ubiquitin-positive frontotemporal dementia linked to chromosome 17q21. *Nature* 2006; **442**: 920–924.
10. Watts GDJ, Wymer J, Kovach MJ *et al.* Inclusion body myopathy associated with Paget disease of bone and frontotemporal dementia is caused by mutant valosin-containing protein. *Nat Genet* 2004; **36**: 377–381.
11. Morita M, Al-Chalabi A, Anderson PM *et al.* A locus on chromosome 9p confers susceptibility to ALS and frontotemporal dementia. *Neurology* 2006; **66**: 839–844.
12. Vance C, Al-Chalabi A, Ruddy D *et al.* Familial amyotrophic lateral sclerosis with frontotemporal dementia is linked to a locus on chromosome 9p13.2-21.3. *Brain* 2006; **129**: 868–875.
13. Yokoseki A, Shiga A, Tan CF *et al.* TDP-43 Mutation in Familial Amyotrophic Lateral Sclerosis. *Ann Neurol* 2008; **63**: 538–542.
14. Gitcho MA, Baloh RH, Chakraverty S *et al.* TDP-43 A315T mutation in familial motor neuron disease. *Ann Neurol* 2008; **63**: 535–538.
15. Sreedharan J, Blair IP, Tripathi VB *et al.* TDP-43 mutations in familial and sporadic amyotrophic lateral sclerosis. *Science* 2008; **319**: 1668–1672.
16. Kabashi E, Valdmanis PN, Dion P *et al.* TARDBP mutations in individuals with sporadic and familial amyotrophic lateral sclerosis. *Nat Genet* 2008; **40**: 572–574.
17. Van Deerlin VM, Leverenz JB, Bekris LM *et al.* TARDBP mutations in amyotrophic lateral sclerosis with TDP-43 neuropathology: a genetic and histopathological analysis. *Lancet Neurol* 2008; **7**: 409–416.
18. Ou SH, Wu F, Harrich D, Garcia-Martinez LF, Gaynor RB. Cloning and characterization of a novel cellular protein, TDP-43, that binds to human immunodeficiency virus type 1 TAR DNA sequence motifs. *J Virol* 1995; **69**: 3584–3596.
19. Wang H-Y, Wang I-F, Bose J, Shen C-KJ. Structural diversity and functional implications of the eukaryotic TDP gene family. *Genomics* 2004; **83**: 130–139.
20. Abhyankar MM, Urekar C, Reddi PP. A novel CpG-free vertebrate insulator silences the testis-specific SP-10 gene in somatic tissues: role for TDP-43 in insulator function. *J Biol Chem* 2007; **282**: 36143–36154.
21. Strong MJ, Volkening K, Hammond R *et al.* TDP43 is a human low molecular weight neurofilament (hNFL) mRNA-binding protein. *Mol Cell Neurosci* 2007; **35**: 320–327.
22. Ayala YM, Misteli T, Baralle FE. TDP-43 regulates retinoblastoma protein phosphorylation through the repression of cyclin-dependent kinase 6 expression. *Proc Natl Acad Sci USA* 2008; **105**: 3785–3789.
23. Buratti E, Baralle FE. Characterization and functional implications of the RNA binding properties of nuclear factor TDP-43, a novel splicing regulator of CFTR exon 9. *J Biol Chem* 2001; **276**: 36337–36343.
24. Buratti E, Dork T, Zuccato E, Pagani F, Romano M, Baralle FE. Nuclear factor TDP-43 and SR proteins promote in vitro and in vivo CFTR exon 9 skipping. *EMBO J* 2001; **20**: 1774–1784.
25. Mercado PA, Ayala YM, Romano M, Buratti E, Baralle FE. Depletion of TDP 43 overrides the need for exonic and intronic splicing enhancers in the human apoA-II gene. *Nucleic Acids Res* 2005; **33**: 6000–6010.
26. Bose JK, Wang IF, Hung L, Tarn WY, Shen CK. TDP-43 overexpression enhances exon 7 inclusion

during the survival of motor neuron pre-mRNA splicing. *J Biol Chem* 2008; **283**: 28852–28859.
27. Buratti E, Brindisi A, Giombi M, Tisminetzky S, Ayala YM, Baralle FE. TDP-43 binds heterogeneous nuclear ribonucleoprotein A/B through its C-terminal tail. *J Biol Chem* 2005; **280**: 37572–37584.
28. Buratti E, Baralle FE. Multiple roles of TDP-43 in gene expression, splicing regulation, and human disease. *Front Biosci* 2008; **13**: 867–878.
29. Mackenzie IRA, Baborie A, Pickering-Brown S *et al.* Heterogeneity of ubiquitin pathology in frontotemporal lobar degeneration: classification and relation to clinical phenotype. *Acta Neuropathol (Berl)* 2006; **112**: 539–549.
30. Mackenzie IRA, Baker M, Pickering-Brown S *et al.* The neuropathology of frontotemporal lobar degeneration caused by mutations in the progranulin gene. *Brain* 2006; **129**: 3081–3090.
31. Sampathu DM, Neumann M, Kwong LK *et al.* Pathological heterogeneity of frontotemporal lobar degeneration with ubiquitin-positive inclusions delineated by ubiquitin immunohistochemistry and novel monoclonal antibodies. *Am J Pathol* 2006; **169**: 1343–1352.
32. Cairns NJ, Bigio EH, Mackenzie IR *et al.* Neuropathologic diagnostic and nosologic criteria for frontotemporal lobar degeneration: consensus of the Consortium for Frontotemporal Lobar Degeneration. *Acta Neuropathol (Berl)* 2007; **114**: 5–22.
33. Snowden J, Neary D, Mann D. Frontotemporal lobar degeneration: clinical and pathological relationships. *Acta Neuropathol (Berl)* 2007; **114**: 31–38.
34. Kwong LK, Uryu K, Trojanowski JQ, Lee VM. TDP-43 proteinopathies: neurodegenerative protein misfolding diseases without amyloidosis. *Neurosignals* 2008; **16**: 41–51.
35. Geser F, Brandmeir NJ, Kwong LK *et al.* Evidence of multisystem disorder in whole-brain map of pathological TDP-43 in amyotrophic lateral sclerosis. *Arch Neurol* 2008; **65**: 636–641.
36. Nishihira Y, Tan CF, Hoshi Y *et al.* Sporadic amyotrophic lateral sclerosis of long duration is associated with relatively mild TDP-43 pathology. *Acta Neuropathol* 2009; **117**: 45–53.
37. Hasegawa M, Arai T, Nonaka T *et al.* Phosphorylated TDP-43 in frontotemporal lobar degeneration and amyotrophic lateral sclerosis. *Ann Neurol* 2008; **64**: 60–70.
38. Inukai Y, Nonaka T, Arai T *et al.* Abnormal phosphorylation of Ser409/410 of TDP-43 in FTLD-U and ALS. *FEBS Lett* 2008; **582**: 2899–2904.
39. Arai T, Ikeda K, Akiyama H *et al.* Identification of amino-terminally cleaved tau fragments that distinguish progressive supranuclear palsy from corticobasal degeneration. *Ann Neurol* 2004; **55**: 72–79.
40. Hasegawa M, Arai T, Akiyama H *et al.* TDP-43 is deposited in the Guam parkinsonism-dementia complex brains. *Brain* 2007; **130**: 1386–1394.
41. Geser F, Winton MJ, Kwong LK *et al.* Pathological TDP-43 in parkinsonism-dementia complex and amyotrophic lateral sclerosis of Guam. *Acta Neuropathol (Berl)* 2007; **115**: 133–145.
42. Miklossy J, Steele JC, Yu S *et al.* Enduring involvement of tau, beta-amyloid, alpha-synuclein, ubiquitin and TDP-43 pathology in the amyotrophic lateral sclerosis/parkinsonism-dementia complex of Guam (ALS/PDC). *Acta Neuropathol* 2008; **116**: 625–637.
43. Amador-Ortiz C, Lin WL, Ahmed Z *et al.* TDP-43 immunoreactivity in hippocampal sclerosis and Alzheimer's disease. *Ann Neurol* 2007; **61**: 435–445.
44. Higashi S, Iseki E, Yamamoto R *et al.* Concurrence of TDP-43, tau and alpha-synuclein pathology in brains of Alzheimer's disease and dementia with Lewy bodies. *Brain Res* 2007; **1184**: 284–294.
45. Hu WT, Josephs KA, Knopman DS *et al.* Temporal lobar predominance of TDP-43 neuronal cytoplasmic inclusions in Alzheimer disease. *Acta Neuropathol* 2008; **116**: 215–220.
46. Josephs KA, Whitwell JL, Knopman DS *et al.* Abnormal TDP-43 immunoreactivity in AD modifies clinicopathologic and radiologic phenotype. *Neurology* 2008; **70**: 1850–1857.
47. Uryu K, Nakashima-Yasuda H, Forman MS *et al.* Concomitant TAR-DNA-binding protein 43 pathology is present in Alzheimer disease and corticobasal degeneration but not in other tauopathies. *J Neuropathol Exp Neurol* 2008; **67**: 555–564.
48. Nakashima-Yasuda H, Uryu K, Robinson J *et al.* Co-morbidity of TDP-43 proteinopathy in Lewy body related diseases. *Acta Neuropathol (Berl)* 2007; **114**: 221–229.
49. Freeman SH, Spires-Jones T, Hyman BT, Growdon JH, Frosch MP. TAR-DNA binding protein 43 in Pick disease. *J Neuropathol Exp Neurol* 2008; **67**: 62–67.
50. Lin WL, Dickson DW. Ultrastructural localization of TDP-43 in filamentous neuronal inclusions in various neurodegenerative diseases. *Acta Neuropathol* 2008; **116**: 205–213.
51. Arai T, Mackenzie IR, Hasegawa M *et al.* Phosphorylated TDP-43 in Alzheimer's disease and dementia with Lewy bodies. *Acta Neuropathol* 2009; **117**: 125–136.
52. Schwab C, Arai T, Hasegawa M, Akiyama H, Yu S, McGeer PL. TDP-43 pathology in familial British dementia. *Acta Neuropathol* 2009; **118**:303–311.
53. Fujishiro H, Uchikado H, Arai T *et al.* Accumulation of phosphorylated TDP-43 in brains of patients with